ISSN 1063-7788, Physics of Atomic Nuclei, 2017, Vol. 80, No. 7, pp. 1227–1248. © Pleiades Publishing, Ltd., 2017.
Original Russian Text © I.V. Aleksandrova, E.R. Koresheva, I.E. Koshelev, O.N. Krokhin, A.I. Nikitenko, I.E. Osipov, 2016, published in Voprosy Atomnoi Nauki i Tekhniki, Seriya: Termoyadernyi Sintez, 2016, Vol. 39, No. 1, pp. 30–54.

Cryogenic Hydrogen Fuel for Controlled Inertial Confinement Fusion (Cryogenic Target Factory Concept Based on FST-Layering Method)

I. V. Aleksandrova[a], E. R. Koresheva[a, b, *], I. E. Koshelev[a], O. N. Krokhin[a, b], A. I. Nikitenko[a], and I. E. Osipov[c]

[a] *Lebedev Physical Institute, Russian Academy of Sciences, Moscow, Russia*
[b] *National Research Nuclear University MEPhI (Moscow Engineering Physics Institute), Moscow, Russia*
[c] *Inter RAO UES Power Efficiency Centre, Moscow, Russia*
**e-mail: elena.koresheva@gmail.com*

Received December 28, 2015

Abstract—A central element of a power plant based on inertial confinement fusion (ICF) is a target with cryogenic hydrogen fuel that should be delivered to the center of a reactor chamber with a high accuracy and repetition rate. Therefore, a cryogenic target factory (CTF) is an integral part of any ICF reactor. A promising way to solve this problem consists in the FST layering method developed at the Lebedev Physical Institute (LPI). This method (rapid fuel layering inside moving free-standing targets) is unique, having no analogs in the world. The further development of FST-layering technologies is implemented in the scope of the LPI program for the creation of a modular CTF and commercialization of the obtained results. In this report, we discuss our concept of CTF (CTF-LPI) that exhibits the following distinctive features: using a FST-layering technology for the elaboration of an in-line production of cryogenic targets, using an effect of quantum levitation of high-temperature superconductors (HTSCs) in magnetic field for noncontacting manipulation, transport, and positioning of the free-standing cryogenic targets, as well as in using a Fourier holography technique for an on-line characterization and tracking of the targets flying into the reactor chamber. The results of original experimental and theoretical investigations performed at LPI indicate that the existing and developing target fabrication capabilities and technologies can be applied to ICF target production. The unique scientific, engineering, and technological base developed in Russia at LPI allows one to make a CTF-LPI prototype for mass production of targets and delivery thereof at the required velocity into the ICF reactor chamber.

Keywords: inertial confinement fusion, free-standing target (FST), in-line production, high-temperature superconductors, magnetic levitation (maglev), Fourier holography, cryogenic target factory

DOI: 10.1134/S1063778817070018

INTRODUCTION

Controlled nuclear fusion (CNF) is now at such a stage where the development of reactor technologies and the construction of a demonstration reactor become topical problems. CNF is developing in two main directions that differ from each other in the way of confinement of hot thermonuclear plasma:

—Magnetic confinement fusion (MCF), where the heated fuel plasma is held for a long time in a quasi-static manner by means of a strong magnetic field in such installations as a tokamak and stellarator. At the same time, a MCF reactor can operate in an almost steady-state mode. The feasibility of the MCF-based approach should be first demonstrated at the international tokamak ITER, the construction of which started in 2008 in the south of France.

—Inertial confinement fusion (ICF), wherein, in contrast to the MCF, plasma is confined by nothing except its own inertia. All the nuclear fusion reactions occur within a short period of time, measured in fractions of a nanosecond. In fact, in the case of the controlled ICF, we deal with a sequence of controlled thermonuclear microexplosions. Therefore, the ICF reactor would operate in a pulsed mode, rather than in a steady-state one, as takes place in the case of the MCF. To demonstrate the energy of nuclear fusion obtained according to the ICF scheme, experimental laboratory facilities have been built in many countries of the world (see [1] and a list of references therein). The purpose of their work is to demonstrate the technical breakeven of ICF, when the energy released in thermonuclear reactions exceeds all the consumed energy. At present, a so-called scientific breakeven has been demonstrated, i.e., the energy released in thermonuclear reactions for the first time exceeded the energy consumed by the compression and heating of the fuel.

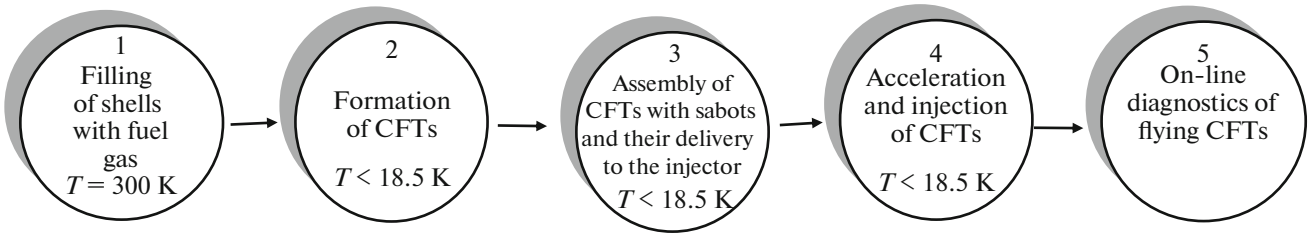

Fig. 1. The main stages of CTF operation.

To obtain the desired positive yield owing to the compression and heating of fuel in the ICF reactor, it is necessary that the fuel be supplied to the center of the reactor chamber at a rate of ~10 Hz (in the case of a laser or heavy-ion driver) or 0.1 Hz (in the case of Z-pinch) [1]. Therefore, at present, research areas that are directly related to the development of rep-rated methods for the formation of cryogenic targets and the creation of a pilot plant—cryogenic target factory—to demonstrate the mass production at the required rates are under way. In this paper, a conceptually new approach to the posed problem based on a rapid formation of a solid fuel layer within moving free-standing targets (FST-layering method) is discussed [1–4], and a review of the main results is given, as well as the results of the latest studies obtained within this approach on the key issues of the development of a CTF for ICF reactors with a laser driver.

CRYOGENIC TARGET FACTORY IN THE CONCEPT OF LPI

A cryogenic fuel target represents a system of embedded spherical layers, the simplest variant of which involves a polymer shell and a cryogenic layer of fuel. The quality requirements for such layers are quite high: deviations ε_1 from sphericity and the concentricity should not exceed 1%; local inhomogeneities on the surface of the fuel layer ε_2 (the roughness or smoothness of the layer) should not exceed 1 μm [5]. The reactor operating conditions exclude any possibility of CFT formation directly in the target irradiation zone, as is done now in experimental laser facilities. Therefore, one of the most important tasks in the program of reactor technology development consists in the CFT quality survival in the course of delivery into the zone of fusion [6]. This means that the cryogenic hydrogen fuel inside a CFT should have such a structure (ultrafine or nanocrystalline) [1, 2] which would provide the survival of the fuel layer quality in the course of the target acceleration, injection, and transport through the ICF reactor chamber. The main stages of the CTF operation in a closed production cycle and of the CFT delivery into the fusion zone are shown in Fig. 1. At the same time, let us emphasize that the fundamental condition that allows one to perform the repeatable production just consists in the use of unmounted CFTs, i.e., free-standing ones not being fixed on any suspension.

Let us make one more important remark. In developing any reactor technology, the requirement is to minimize the tritium inventories in the subsystems of the ICF reactor and hence in the CTF subsystems. The best is the technological solution that provides minimum time and space scales of each stage of production of CFT.

At present, it is possible to solve the entire complex of tasks only on the basis of the FST-layering method (the formation of a fuel layer inside moving free-standing shells) proposed and developed at LPI [1–4]. Such an approach opens the possibility for the development of a fundamentally novel energy-efficient technology for the production of environmentally friendly fuel to generate electricity and heat according to the ICF scheme. At the same time, it should be emphasized that the efficiency of a thermonuclear power plant can be provided on the basis of several simultaneously operating reactors, namely, one driver–one CTF–N reactors ($N > 5$). And for this, it is necessary that the CTF carry out the production of targets in-line, or, in other words, in a "pipeline" manner, which at present is possible only in the course of the implementation of a FST-layering method.

For comparison, it should be noted that, in foreign laboratories, researchers traditionally developed technologies for the production of a target attached to some material suspension (a thread, capillary, cone, etc.). This approach is not applicable to ICF power stations, since the delivery of such a target is not feasible in the high rep-rate mode. In addition, the traditional technologies are characterized by a high production cost, more than $1000 per 1 CFT [7]. Currently, the FST-layering method is the cheapest technology in the world (the construction of a FST system is 100 times cheaper than any other target system based on traditional technologies) [1]. This is a key point in the development of reactor technologies, since the cost of CFT is the main factor that determines the economy of a power plant based on ICF [1, 7]. That is why the development of cost-effective technologies for CFT production would allow one to control the cost of 1 kWh in the energy market in the future.

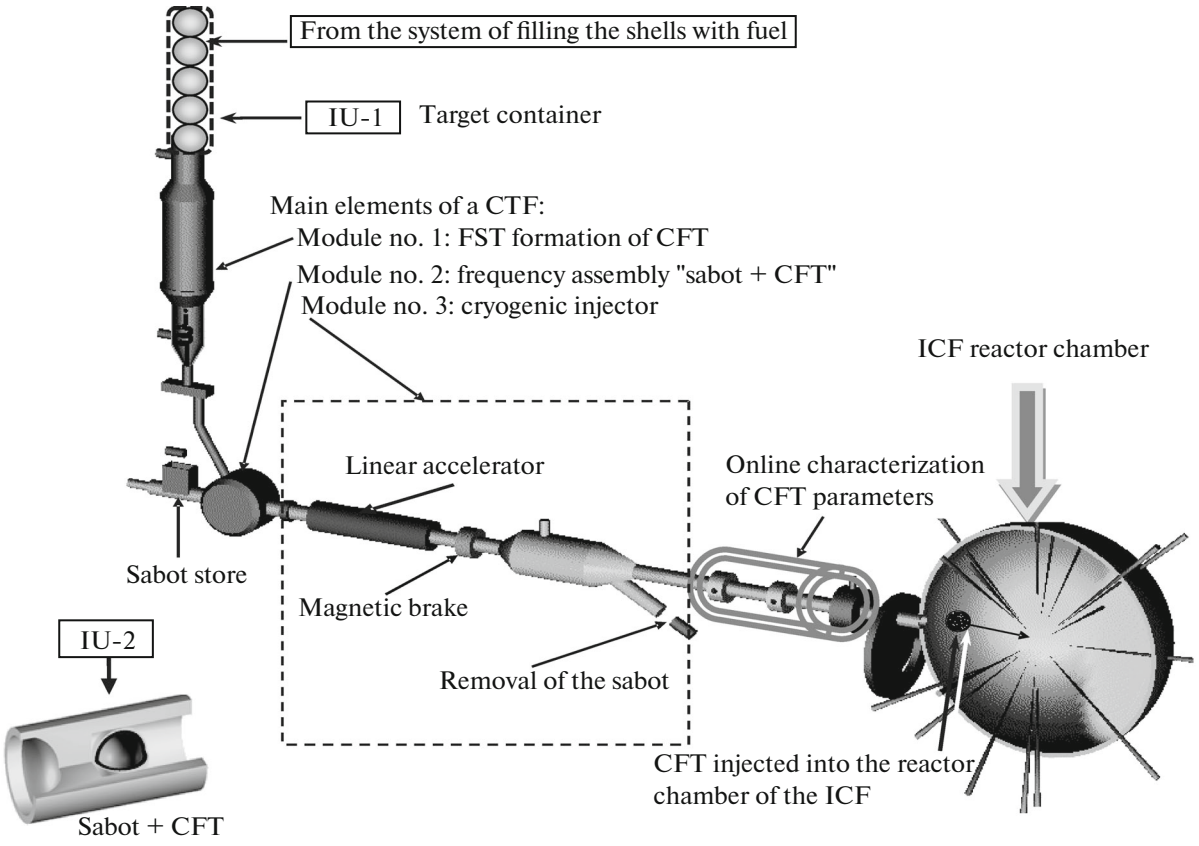

Fig. 2. Schematic diagram of CTF in the concept of LPI (CTF-LPI).

A schematic diagram of the CTF in the concept of LPI (CTF-LPI) is shown in Fig. 2. The scheme involves the following main modular blocks:

—module no. 1: FST-layering module (LM) for in-line production of free-standing CFT with a line productivity starting from 500 000 and more CFTs per day (Fig. 3);

—module no. 2: assembling module (AssM) for assembling CFTs with special carriers (so-called sabots), working with a rate up to 10 CFTs per 1 s;

—module no. 3: acceleration module (AccM) for sabot and CFT acceleration to a velocity of 200–400 m/s and CFT injection into the reactor chamber with a required frequency.

Important elements of the CTF are interface units (IU) that perform interfacing the modules together. In the CTF-LPI, the main interface units are the following:

—IU-1: target container (TC) (see Figs. 2 and 3) for supplying a shells batch with gaseous fuel from the filling system to the FST-layering module (module no. 1);

—IU-2: sabot for feeding CFT to the acceleration module (module no. 3).

The control element of the CTF is a system for on-line characterization and tracking of the targets flying into the reactor chamber on the basis of Fourier holography.

The order of the CTF-LPI operation is as follows.

TC transportation with an array of filled shells from the filling system to the FST-formation module (module no. 1). Filling of the shells with fuel is carried out either via diffusion [8] or via injection [5]. The FST-layering method works with the shells that are filled using either of the methods. A diffusion filling system has been developed at LPI which system provides an internal fuel gas pressure of up to 1000 atm at 300 K within the thin-walled polymeric shells [8]. The idea of its operation is based on a continuous (or quasicontinuous) increase in pressure in the filling chamber in such a way that the pressure difference inside and outside the shell does not exceed a certain value. At the same time, an automatic control the system parameters is carried out.

The TC is an interface unit for filling the batch of free-standing shells with gaseous fuel, which is then transferred to module no. 1 to integrate into a single system.

CFT formation via the FST-layering method, i.e., the formation of a uniform isotropic ultrafine fuel layer inside the moving free-standing shells in module no. 1. This can be achieved through the implementation of high

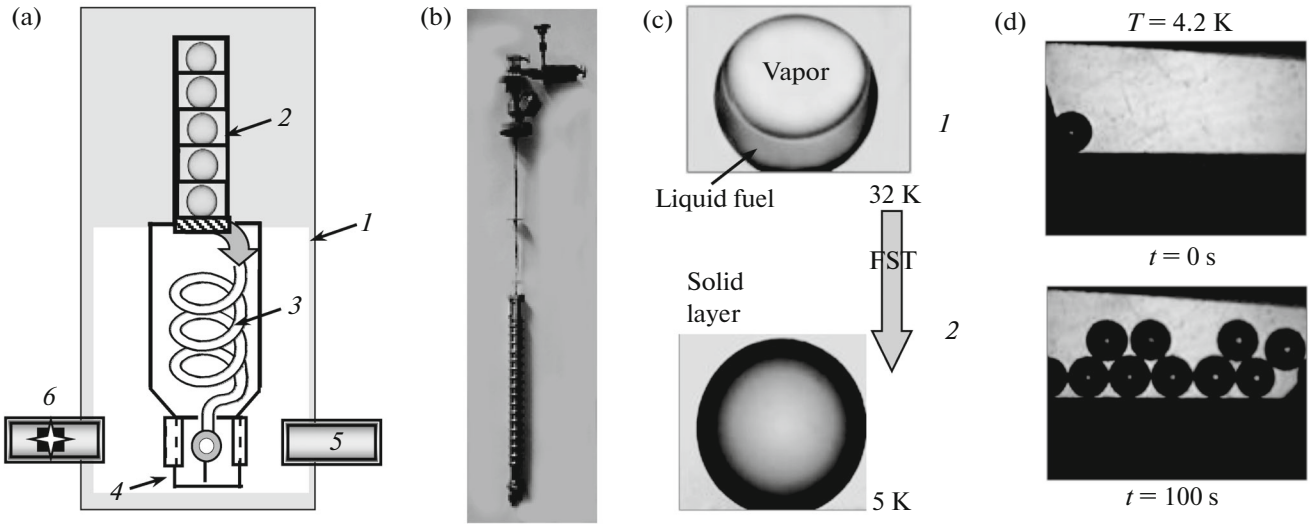

Fig. 3. The FST-layering method provides a rapid formation and symmetrization of solid ultrafine fuel layers in moving shells: (a) FST module design ((*1*) cryostat, (*2*) TC, (*3*) LC, (*4*) TCh, (*5*) video tomograph, (*6*) probing radiation); (b) experimental LC in the form of a single spiral; (c) shell before the beginning of FST-layer formation (fuel in the state "sag liquid + vapor" (*1*)), CFT after FST formation (symmetrical solid layer (*2*)); (d) injection of finished CFT from LC into TCh at $T = 4.2$ K.

cooling rates (from 1 to 50 K/s), which allows one to obtain disordered structures with a high defect density, i.e., an isotropic medium, or so-called ultrafine layers with a fine-grained or nanocrystalline structure. The stabilization of the obtained structures is achieved owing to the introduction of alloying additives into the fuel composition. Such layers belong to the class of layers that are promising for the production of cryogenic targets with a required quality and for the target survival in the course of its delivery to the chamber of an ICF reactor [2–4].

The cycle of CFT formation in module no. 1 is implemented as follows (see Fig. 3). The shells with liquid (or gaseous) fuel located in the TC are injected into the layering channel (LC) that represents a special insert in the cryostat in the form of an evacuated spiral tube with cooled walls (see Figs. 3a–3c). In the LC, the shells with fuel move in rapid succession, one after another, which provides a rep-rate injection of the finished CFTs into the test chamber (TCh, see Fig. 3d).

Two physical principles form the basis of the FST-layering method (see Fig. 3c). They are a dynamic symmetrization of the liquid layer caused by a free CFT rotation as it moves in the LC and a freezing of fuel on the inner surface of the shell owing to the contact thermal conductivity between the moving shell and cold LC wall.

It should be noted that module no. 1 operates simultaneously with a batch of free-standing targets (according to the reactor technologies). At the same time, the targets remain free-standing at all the stages of production. The implementation of high cooling rates (from 1 to 50 K/s) [1–4] in comparison with the traditional methods of layer formation (~3×10^{-5} K/s) [1, 5] meets the requirements for minimizing the radioactive tritium inventories in the CTF, i.e., for minimizing the time and space scales of each stage of CFT production owing to the following features of the FST-layering method [1–4]:

—minimum space scale owing to a close packing of free-standing CFT;

—minimum time scale due to a minimum layering time at high cooling rates—less than 15 s (in the case of traditional technologies up to 24 h [5]);

—injection transport of targets between the main functional elements of module no. 1: TC–LC–TCh (no storage of targets in intermediate stages).

Thus, the FST-layering method is a promising way to solve the problem of the in-line formation and injection transport of CFTs as well as for using in future power plants for process engineering (Fig. 4).

Assembling "Sabot + CFT" ensembles using a revolver mechanism in module no. 2. A sabot represents a protective carrier capsule that performs the two following functions: transmitting the momentum to a CFT under acceleration to a required injection rate, as well as protecting the CFTs from destruction as a result of overloads occurring at the acceleration stage.

Preliminary acceleration of "Sabot + CFT" ensembles to a velocity ranging from 1 to 8 m/s. The ensemble "Sabot + CFT" is extracted from a drum of the revolver mechanism of module no. 2 owing to the action of a solenoidal magnetic field on the magnetoactive material of the sabot. As a result, the ensemble is pre-accelerated to a velocity ranging from 1 to 8 m/s and moves along the barrel toward a starting position in the cryogenic injector (module no. 3).

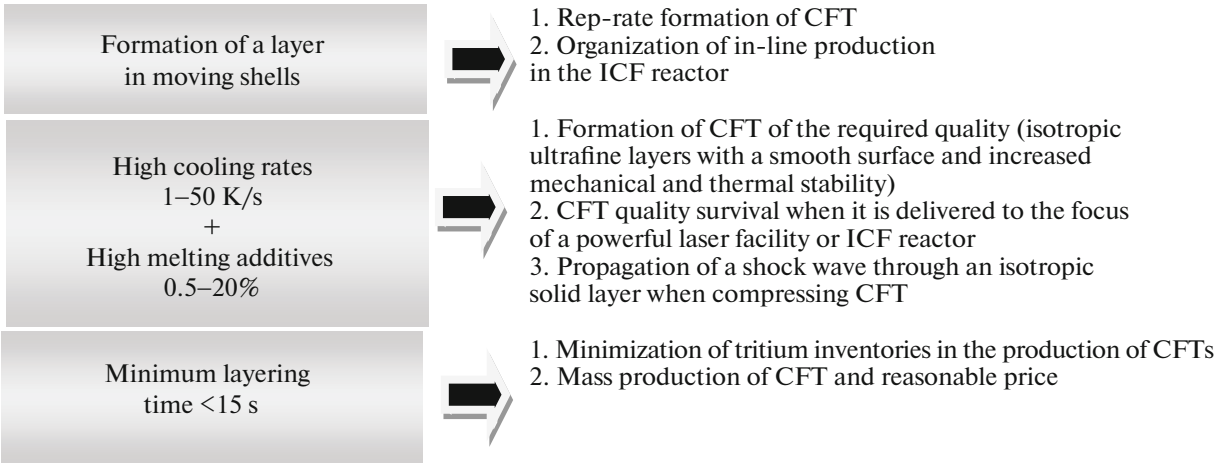

Fig. 4. Characteristic parameters of the FST-layering method proposed and developed at LPI for in-line production and injection transport of CFT.

Acceleration of "Sabot + CFT" ensembles in module No. 3 to a velocity from 200 to 400 m/s. In a cryogenic injector, the ensemble "Sabot + CFT" accelerates to the required velocity, after which the CFT is separated from the sabot and injected into the reactor chamber and then flies into the focus of the powerful laser facility. It should be noted that module no. 3 also includes a trajectory correction system based on the quantum HTSC levitation effect, as well as a braking system for the separation of the Sabot + CFT ensemble and the subsequent removal of the sabot.

On-line characterization of CFT quality parameters and the trajectory of CFT motion can operate in two variants: CFT monitoring at the output of the injector (if such a procedure is necessary), as well as at the stage of CFT flight in the ICF reactor chamber.

Summary. An essential part of the ICF reactor is a CTF, the purpose of which consists in the mass production of free-standing CFTs and their rep-rate delivery to the focus of a powerful laser facility. The key tasks in the construction of the CTF consist in choosing an efficient method for the formation of CFTs and making an appropriate device for their production, in the development of a system for precise and high rep-rate delivery of free-standing CFTs to the laser irradiation zone, and in the development of methods for the on-line characterization of injected CFT. The solution of the first problem in the LPI concept consisting in the application of the FST-layering method (module no. 1) is presented in [3, 4] (see also the list of references therein), whereas the second and the third problems are discussed in detail later. It should be emphasized that novel technologies based on the use of moving free-standing targets (the FST-layering method, LPI, Fig. 5), allow one to substantially simplify technological solutions and to significantly reduce the cost of development.

DELIVERY STAGE—REQUIREMENTS FOR THE FUEL LAYER STRUCTURE

The production of targets of the reactor class requires the development of such methods of layer formation that would satisfy the requirements for the physics of target compression, namely: the cryogenic fuel layer must be isotropic so that the required density and temperatures for the nuclear fusion are achieved in the course of the CFT compression [9].

Let us recall that the use of nanostructured materials allows one to reduce the sensitivity of the samples with respect to thermal and mechanical overloads. That is why nanomaterials are recommended for use in the main elements of the ICF reactor, such as the wall of the reactor chamber, the active medium of a solid-state laser, and the wall of a CFT shell [1]. Of late, there has been an urgent question concerning the development of novel technologies that make it possible to obtain a fuel layer in the nanostructured state [2, 9]. It is just the structure of the fuel layer that determines its quality at the stage of CFT formation. The studies in this direction are being intensively conducted now in Russia, Spain, and the United States [1]. The authors of [9] directly emphasized the necessity of the formation of nanocrystalline targets for the NIF class installation: "Our results indicate that just the nanocrystalline layers guarantee small fluctuations in the shock wave front, which minimizes the occurrence of dangerous instabilities in the compression of NIF targets."

However, in order to implement the ICF energy scheme, it is necessary not only to form the required fuel structure inside the target but also to provide the structural and phase stabilization in the course of target delivery to the laser focus in the ICF reactor. The distinctive feature of the delivery process consists in the requirements for the delivery rate (~10 Hz), delivery accuracy (±20 μm), and the temperature mode of

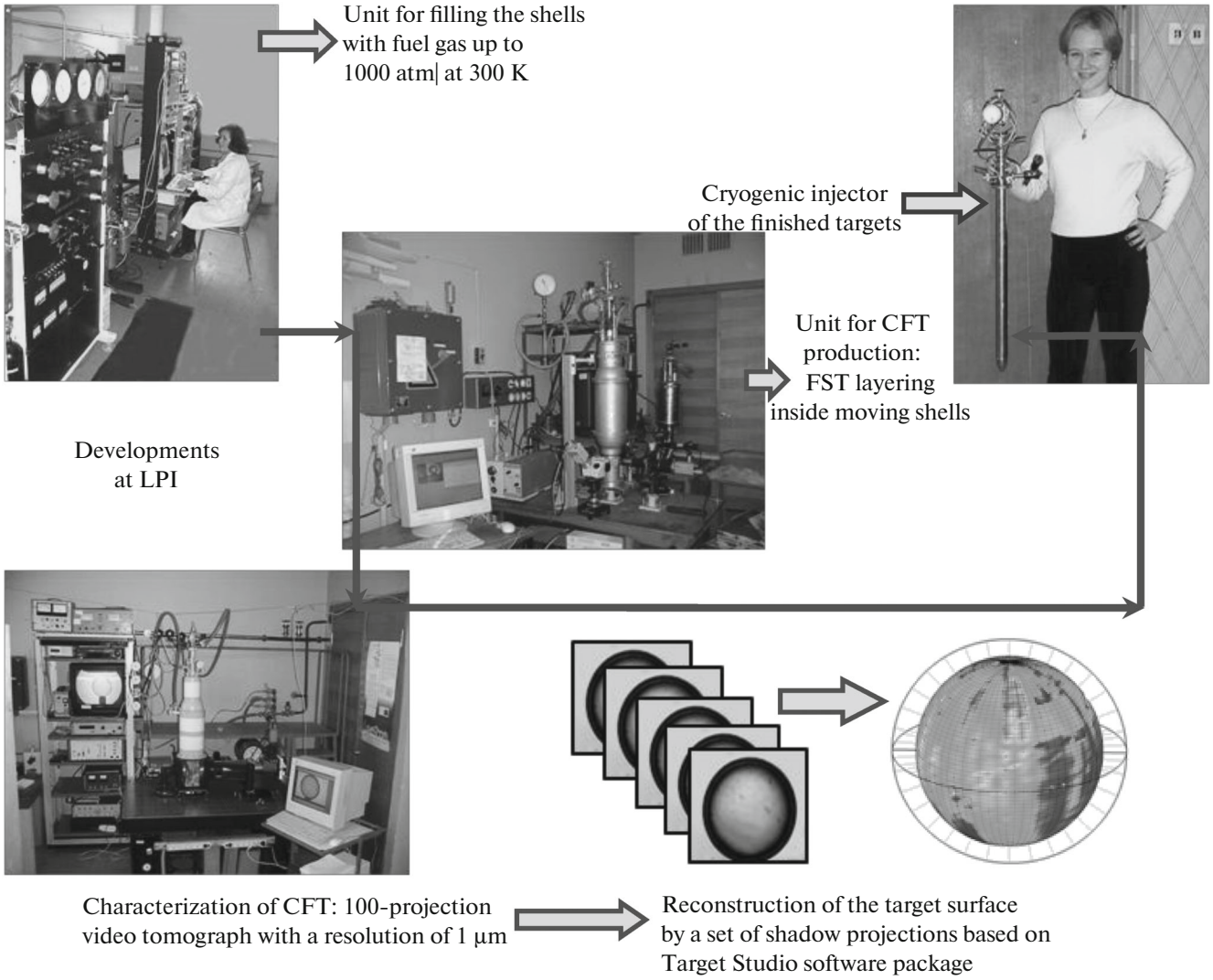

Fig. 5. Main elements of CTF based on the FST-layering method were tested on prototypes created at the LPI that allows one to significantly reduce the risks in its development.

delivery. A CFT (a hollow polymeric shell with a spherical layer of hydrogen fuel on its inner surface) should have a temperature not exceeding 18.5 K at the moment of laser irradiation. At the same time, the wall temperature of the reactor chamber itself can reach significant values. So, for example, for the chamber of a SOMBRERO reactor, this value amounts to 1758 K [10]. In addition, at the stage of acceleration in the injector, the permissible overloads on CFT can be as high as 1000 *g* [11].

Under these conditions, the study of the evolution of the structure of cryogenic fuel layers under the influence of various external factors is one of the most important tasks in the general problem of ICF. In this section, we consider a question concerning the structural and phase stabilization of nuclear fuel under the action of thermal radiation from the walls of the reactor chamber in order to understand what requirements for the fuel structure proceeding from the features of the process of CFT delivery.

Delivery stage. The important point in the delivery of targets to the focus of a powerful laser facility consists in the survival of cryogenic fuel layers. The delivery process involves the acceleration stage in the injector and the stage of target flight inside the chamber. The fundamentally unavoidable sources of the mechanical and thermal target destruction at these stages consist in overloads in the course of acceleration and heat inflows from the radiation of the chamber walls and hot residual gas.

Decreasing the target injection rate into the reactor chamber makes it possible to reduce overloads and thereby to reduce the probability of mechanical destruction of the target. However, the lower the injection rate, the longer the CFT is under the influence of thermal overloads, which threaten the cryo-

genic layer with thermal destruction, i.e., with growing roughness (high perturbation modes) and variability of the thickness (low perturbation modes) over and above permissible values. Therefore, to deliver CFT without destruction, it is necessary to perform a detailed study, whose subject is an effect of the degradation of the fuel layer with different internal structure under the action of thermal radiation from the walls of the chamber wherein the CFT moves.

The survival of cryogenic hydrogen fuel layers exposed to external influences depends on the structure of the layer. Considering this issue, we were guided by the fact that, in the equilibrium state, the solid isotopes of hydrogen consist of anisotropic molecular crystals. It was found by the authors of [12] that the anisotropy in the sound velocity is inherent in the hexagonal close-packed (HCP) phases of hydrogen isotopes. For hydrogen (H_2) and deuterium (D_2), the anisotropy amounts to about 20% (longitudinal sound) and 33% (transverse sound). Since in accordance with the Debye theory the lattice thermal conductivity is directly proportional to the velocity of sound, then even in the case of a uniform thermal load on the target surface (to refer to the transport of the target into a reactor chamber with hot walls), there is a difference in the radial temperature gradient in the case of an anisotropic cryogenic layer. This is the reason for a spherically asymmetric sublimation of the fuel substance, which leads to the layer degradation in terms of roughness and thickness during delivery of an originally ideal target to the focus of a laser facility.

The studies on the problem were begun by the authors of [13] and continued in [14, 15]. To date, codes have been optimized and numerical modeling of the fuel layer degradation has been carried out for heating of the cryogenic target in the reactor chamber with warm walls for the following two cases of our interest:

—Isotropic ultrafine layer. The cooling rate values inherent in the FST-layering method ($q = 1$–50 K/s) promote the formation of extremely disordered structures with a high defect density, i.e., the formation of an isotropic medium. In an isotropic layer, the thermal conductivity coefficient k_s does not depend on the spatial coordinates.

—Anisotropic molecular crystals (real single crystals or coarse-grained crystalline, the cooling rate $q \sim 3 \times 10^{-5}$ K/s). The formation of a fuel layer in an anisotropic crystalline state is typical of traditional methods for the CFT production. In this case, the thermal conductivity coefficient of the layer depends on the spatial coordinates, whereas the experiments on the compression of such targets confirm a high sensitivity of anisotropic fuel with respect to external thermal impact on the CFT [5].

Formulation of the problem. Let us try to trace the thermal history of a target with a different degree of anisotropy of the layer in the course of its flight in the reactor chamber with warm walls. In the system of spherical coordinates r, θ, ϕ, the thermal conductivity coefficient for an anisotropic layer can be written in the following form:

$$k_1 = k_s(1 + \xi_1(\varphi, \theta)); \quad k_2 = k_s(1 + \xi_2(\varphi, \theta));$$
$$k_3 = k_s(1 + \xi_3(\varphi, \theta)),$$

where ξ_n ($n = 1, 2, 3$) is a dimensionless function that describes the dependence of the thermal conductivity on the direction.

First of all, let us formalize the problem of gas sublimation. Let $T_m(r, t)$, $k_m(T)$, $c_m(t)$, and $\rho_m(T)$ denote the temperature, thermal conductivity, heat capacity, and density of target components. Index m = sh, s, g, where sh and s refer to the polymeric shell and the cryogenic layer, respectively, and g refers to the gas. In an anisotropic (crystalline) cryogenic layer, the heat flux in spherical coordinates is given by vector $\mathbf{j}_s$:

$$\mathbf{j}_s = -\left(k_1 \frac{\partial T_s}{\partial r}, k_2 \frac{\partial T_s}{r\partial\theta}, k_3 \frac{\partial T_s}{r\sin\theta\partial\varphi}\right).$$

Here $T_s(r, \theta, \varphi, t)$ is the temperature in the cryogenic layer at the moment of time t. The dynamics of the temperature in the shell is described by the equation of thermal conductivity

$$\rho_{sh}c_{sh}(T)\frac{dT_{sh}}{dt} = \alpha_{sh}J_{sh} \tag{1}$$

with the initial condition

$$T_{sh}(0) = T_i. \tag{2}$$

Factor α_{sh} is the radiation absorption coefficient per unit length. The value of J_{sh} in (1) determines the flux of thermal radiation from the wall of the reactor chamber wherein the CFT is located. In this case, the irradiation problem is spherically symmetric, and for the flux value, one can use the Stefan–Boltzmann law

$$J_{sh} = \sigma T_0^4, \tag{3}$$

where σ is the Stefan–Boltzmann constant, T_0 is the temperature of the inner wall of the reactor chamber, and T_i is the initial temperature of the target when it is injected into the reactor chamber (injection temperature). At the interface "shell–cryogenic layer," the temperatures of both media are

$$T_{sh}(t) = T_s(r_1, \theta, \varphi, t). \tag{4}$$

The dynamics of the temperature inside the crystalline layer, in view of the absence of spherical symmetry, has the form

$$\rho_s c_s \frac{\partial T_s}{\partial t} = \alpha_s J_s(r) + \frac{1}{r^2}\frac{\partial}{\partial r}\left((k_1(r,\theta,\varphi)r^2\frac{\partial T_s}{\partial r}\right)$$
$$+ \frac{1}{r^2\sin\theta}\frac{\partial}{\partial\theta}\left(k_2(r,\theta,\varphi)\sin\theta\frac{\partial T_s}{\partial\theta}\right) \tag{5}$$
$$+ \frac{1}{r^2\sin^2\theta}\frac{\partial}{\partial\varphi}\left(k_3(r,\theta,\varphi)\frac{\partial T_s}{\partial\varphi}\right),$$

$$J_s = J_{sh}\exp(-\alpha_{sh}w_{sh} - \alpha_s(r_1 - r)). \quad (6)$$

Here and below, r_0 and r_1 are the outer and inner shell radii, respectively; $w_{sh} = r_0 - r_1$ is the shell thickness; α_s is the absorption coefficient in the layer. Let us write the balance of heat fluxes at the boundary "cryogenic layer + vapor" taking into account the amount of heat necessary for the sublimation of fuel:

$$\left(k_1\frac{\partial T_s}{\partial r} + k_2\frac{\partial T_s}{r^2\partial\theta}\frac{\partial w}{\partial\theta} + k_3\frac{\partial T_s}{r^2\sin^2\theta\partial\varphi}\frac{\partial w}{\partial\varphi}\right)\Bigg|_{r=r_1-w(t)} = -\lambda_s\rho_s\frac{dw}{dt}. \quad (7)$$

Here λ_s is the specific heat of sublimation. The equality of temperatures at the boundary "cryogenic layer + vapor" has the form

$$T_s\big|_{r=r_1-w} = T_g(t). \quad (8)$$

The dependence of the gas temperature on time is explained by the fact that, as a result of sublimation, its density changes and, consequently, the temperature changes too. The sublimation process begins at the moment $t = 0$. Let w_0 be the thickness of the cryogenic layer at the moment $t = 0$. Then the initial conditions are the following:

$$w(0) = w_0; \quad T_g(0) = T_i; \quad T_{sh}(r,0) = f(r); \quad T_s\big|_{t=0} = \psi(r), \quad (9)$$

where $\phi(r)$ and $\psi(r)$ are the initial temperature profiles for the polymeric shell and the cryogenic fuel layer, respectively.

The analysis of this spherically asymmetric system of parabolic equations with a varying boundary (the Stefan problem) was carried out using asymptotic methods for solving singularly perturbed boundary-value problems for parabolic type equations, where the inverse of the layer aspect ratio $\delta^2 = (w/r_0)^2$ (usually $\delta^2 \sim 10^{-2}$) was used as a small parameter. By using this analysis, with some model simplifications, we succeeded in obtaining an ordinary differential equation for the thickness of the cryogenic layer for any values of spherical coordinates θ and φ. It has the form

$$\frac{dw(\varphi,\theta,t)}{dt} = -\gamma_0(\varphi,\theta)\frac{\left(\sqrt{1+\beta t}-1\right)}{w(r_1-w)} - \gamma_1 w\frac{r_1}{r_1-w} + \gamma_2\frac{w^2}{r_1^2(r_1-w)} - \frac{\gamma_3\exp(-\chi^2 t)}{r_1-w}\left\{\cos(\pi w/w_0) + \frac{w_0\sin(\pi w/w_0)}{\pi(r_1-w)}\right\}. \quad (10)$$

The following parameters are used here:

$$\gamma_0 = \frac{k_s(1+\xi_1(\varphi,\theta))}{\lambda_s\rho_s}\frac{\eta_0}{\eta_1}; \quad \gamma_1 = \frac{\alpha_s\sigma T_0^4}{2\lambda_s\rho_s};$$

$$\gamma_2 = \frac{2}{3}r_1^2\gamma_1; \quad \gamma_3 = \frac{4\alpha_s\sigma T_0^4 r_1 w_0}{\pi^2\lambda_s\rho_s};$$

$$\chi^2 = \frac{k_s(1+\xi_1)\pi^2}{c_s\rho_s w_0^2}; \quad \beta = \frac{2\alpha_{sh}\sigma T_0^4}{\rho_{sh}}\frac{\eta_1}{\eta_0^2};$$

$$\eta_0 = c_{sh}(T_i); \quad \eta_1 = \frac{c_{sh}(T_{tp}) - c_{sh}(T_i)}{T_{tp} - T_i},$$

where T_{tp} is the triple point temperature for a given fuel substance.

Equation (10) is solved using a classical Runge-Kutta method that provides a good accuracy with a relatively small amount of computations. In calculations, the temperature-dependent properties of the materials that make up CFT (shell material, hydrogen isotopes) were represented by polynomials of different degrees. The following initial data were used in calculations:

—Classical High Gain Targets (CHGTs)—targets with a high energy yield—were considered. At the present time, several design variants for such a target are under discussion. We will dwell on the variant of CHGT-1 [16], a so-called "Nakai" target. It represents a polymeric shell with a diameter $\varnothing = 4$ mm and a wall thickness $\Delta R = 45$ μm. The thickness of the cryogenic fuel layer is $W = 200$ μm; parameter $\delta^2 = 10^{-2}$. It should be noted that, upon forming the targets, the requirements for the symmetry of the cryogenic layer were always quite strict. Modern representations concerning this question are presented in detail in [5] (parameters ε_1 and ε_2 are shown on page 30).

—A uniform heat flux of radiation from the walls of the SOMBRERO reactor chamber with a temperature of 1758 K falls on the CFT of a CHGT-1-Scale [10]. The heat flux J absorbed in the target material ranges from 5.0 to 0.5 W/cm^2; the target temperature during its injection ranged within $T_i \equiv T_{inj} = 10$–18 K. The obtained results of numerical simulation allow one to estimate the lifetime of the fuel core (i.e, the time until the roughness of the layer exceeds the permissible value determined by relationship $\varepsilon_2 < 1$ μm) and, as a consequence, to determine the conditions of target quality survival upon its injection into the reactor chamber.

The data presented in Table 1 reveal the following regularity: the growth rate of the layer roughness is the smaller, the lower its anisotropy level. For a more detailed analysis, it should be noted that the minimum target flight time in the reactor chamber (injection time Δt_{cc}) is determined by the ratio between the chamber radius (6.5 m for the SOMBRERO type reactor) and the maximum target injection rate (~400 m/s) currently achievable in practice. This time amounts to ~16 ms. If the roughness growth time Δt_{rough} above a permissible value (parameter ε_2) is less than the minimum injection time ($\Delta t_{cc} = 16$ ms), then

even an ideally formed CFT during its flight in the reactor chamber loses its quality and becomes unsuitable for compression according to the ICF scheme.

The analysis of Fig. 6 allows us to make the following important conclusions. A cryogenic layer with an anisotropy $\xi \geq 10\%$ even at a relatively low level of absorbed heat $J = 0.5$ W/cm^2 degrades owing to the growth of its roughness even before the moment when the injected target arrives at the center of the reactor chamber, even at a maximum possible injection velocity of ~400 m/s. For an anisotropic layer at $\xi = 7$–9%, only one possibility remains—target injection at a temperature $T_{inj} = 18$ K. However, in this case, the value of T_{inj} becomes close to the temperature $T_{cc} = 18.5$ K, at which a CFT with a solid DT layer should reach the center of the reactor chamber. In other words, a CFT should be injected into the chamber practically with a limiting velocity of 400 m/s. However, in this case, the dimensions of the injector must be significantly increased at the expense of the increasing in the acceleration length, otherwise the CFT would be destroyed under the action of significant mechanical overloads (the overloads arise in the injector because of the fact that the target acceleration a exceeds the acceleration of gravity g and can reach a value of ~1000 g [11]).

It should be noted that, in the case where the design of the reactor chamber includes residual gas, the injected CFT is exposed not only to the thermal radiation of the chamber walls but also to a convective heating from the side of the hot gas. Under these conditions, the problem of injected target survival becomes even much more complicated.

Summary. Thus, the formation of isotropic ultrafine cryogenic layers represents not only the condition required for obtaining a high-quality fuel but also a condition required for maintaining this quality until the moment of target irradiation. Isotropic ultrafine fuel layers can be attributed to layers with inherent survival features, taking into account their high mechanical and thermal stability. In essence, the matter concerns the production of novel functional fuel-layer structures that exhibit long-lived characteristics of quality. The latter is of great importance for the practical implementation of the requirements for the physics of target compression, as well as for the survival of the fuel layer quality upon delivering the finished CFTs to the ICF reactor chamber.

HTSC APPLICATION TO THE SYSTEM OF CFT DELIVERY INTO ICF REACTOR

To provide a reliable delivery of cryogenic hydrogen fuel, it is necessary to correct either the trajectory of the flying CFT or the direction of laser beam propagation (in accordance with on-line characterization of the CFT trajectory). In the latter case, it is necessary to synchronously control the position of the input

Table 1. Δt_{rough} (ms) as a function of ξ at different values of the absorbed flux

ξ, %	$J = 5$ W/cm^2		$J = 0.5$ W/cm^2	
	D_2	DT	D_2	DT
1	11.7	9.8	27.6	23.0
3	6.4	5.4	15.4	13.0
5	4.7	4.0	11.5	9.7
10	3.0	2.6	7.6	6.5
15	2.4	2.0	6.1	5.1
20	2.0	1.7	5.1	4.4

Injection temperature $T_{inj} = 10$ K.

mirrors of the chamber, the number of which can amount up to 150–200 mirrors. In the course of the development of delivery systems, the most promising variant is the on-line correction of the moving CFT trajectory, which can be realized as a reliable operation at low cost.

One of the approaches proposed in the United States consists in controlling the target trajectory using a laser beam [17]. For this, a CFT should be coated from the outside with an ablation layer of a solidified gas. The directed evaporation of the outer cryogenic layer would compensate the effect of "wind" due to residual gases. In the scope of this scenario, the driver beams arriving at the center of the chamber must be tuned to the trajectory of the target's motion. To obtain a corresponding ablative layer, one can use an original method developed at LPI to apply hardened gases to the outer surface of a moving CFT [18].

Another method for correcting the trajectory of a moving target is based on the use of magnetic lenses. It is assumed that CFT should have an external coating of superconducting material. There are research works known wherein it has been proposed to use superconducting lead as a coating [19, 20]. However, lead has a low superconducting transition temperature ($T_c = 7.2$ K) and a small strength of critical magnetic field ($B_c = 0.08$ T at 0 K, $B_c = 0$ at $T_c = 7.2$ K). Taking into account the fact that a CFT should have a temperature $T \sim 18.5$ K at the moment of irradiation, the use of lead coating is unpromising, since lead at this temperature does not behave as a superconductor.

At LPI, it was proposed to use HTSC materials [21] as a superconducting coating for CFT, whose materials exhibit sufficiently high T_c and B_c values. In particular, the superconducting ceramic based on $YBa_2Cu_3O_{7-X}$ (^{123}Y), whose technology is under development at LPI, exhibits the values of $T_c \simeq 91$–93 K and $B_c > 45$ T.

Another problem in the delivery process consists in the survival of fuel layer parameters until the moment of the CFT irradiation with a pulse of high-power

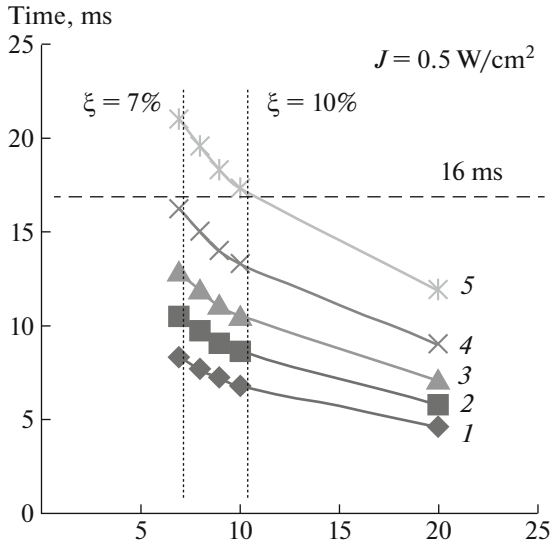

Fig. 6. The time of the growth of the DT layer roughness above the permissible value as a function of its anisotropy at different injection temperatures, T_{inj} = 10 (*1*), 12 (*2*), 14 (*3*), 16 (*4*), 18 K (*5*).

laser. Therefore, the CFT movement is carried out with the use of a protective capsule—a sabot that transmits the momentum to CFT upon its acceleration to the required injection velocities (from 200 to 400 m/s). However, in this case, there occurs a generation of heat due to the friction of the sabot against the guide tube wall of the injector. To exclude this source of the fuel layer destruction, it was proposed to use a sabot trajectory correction system made of HTSC to prevent it from touching the wall of the injector guide tube [22].

Thus, the development of a system for the contactless positioning and transport of CFT represents one of the most important tasks in the overall ICF problem. Preliminary experiments carried out at the Lebedev Physical Institute using the levitation of high-temperature superconductors in a magnetic field confirmed the fruitfulness of this approach.

Preparation of HTSC samples. The purpose of the performed studies consists in the generation of different modes of HTSC sample levitation to test the conditions that can be used to develop the positioning, transport, and CFT trajectory correction systems based on the quantum levitation effect of high-temperature superconductors in a magnetic field.

The HTSC materials allow one to work in the two following directions. They are indirect delivery, where a CFT is preliminarily positioned inside a sabot, and direct delivery, where a CFT moves independently without any carrier.

The implementation of the indirect delivery involves the development of a superconducting sabot, which allows the researchers to avoid any changes in the design of the target. The direct delivery is associated with the application of an external HTSC coating to the surface of a polymeric (CH) shell. This means that the design of the target should be changed. In this case, the application process must have a high degree of repeatability at a high quality level of the HTSC coating itself. In addition, the HTSC coating should satisfy stringent requirements arising from the conditions of target compression physics upon its irradiation with a powerful laser pulse.

The following HTSC samples were tested in the experiments:

—HTSC tablets, as well as fragments of such tablets made of superconducting ceramic $YBa_2Cu_3O_{7-X}$ (^{123}Y, Fig. 7a) produced at LPI.

—CH shells with an outer layer made of a composite material made at LPI (superconducting ^{123}Y powder spread inside the polymer matrix (see Fig. 7b)). The diameter of the shells ∅ ~ 2 mm corresponds to the base target of a HiPER (High Power Laser Energy Research) class [11], designed for performing experiments at the world's first frequency laser facility ($E_1 = 200$ kJ), currently under construction in Europe. Its operation requires the formation and delivery of impact-ignition CFT with a frequency $\nu \geq 1$ Hz.

—HTSC tapes of a SuperOx J-PI-12-20Ag-20Cu type (manufactured by JSC SuperOx, Moscow);

—HTSC sabots (see Fig. 7c) made of ^{123}Y ceramic (produced at LPI);

—HTSC sabots (see Fig. 7d) made of HTSC tapes of a SuperOx J-PI-12-20Ag-20Cu type.

The original tablets made of superconducting ^{123}Y ceramic were fabricated at the Laboratory for Superconductivity of LPI using a solid-phase reaction technique [22]. The ^{123}Y samples had a superconducting transition temperature $T_c = 91$ K at a transition width of 1 K. The values of the lower (B_1) and upper (B_2) critical field amounted to, respectively, $B_1 = 3$ mT (at $T = 17$ K) and $B_2 > 45$ T (at $T = 0$ K). The superconducting ^{123}Y tablets, as well as the fragments of such tablets (see Fig. 7a), were used as substrates or carriers for polymeric shells upon the action of magnetic fields of different configuration.

For obtaining a superconducting powder, the prepared ^{123}Y tablet was ground, triturated, and repeatedly annealed in an oxygen atmosphere at 440°C. At the end of this procedure, the powder was removed from the furnace, and then it was used in levitation experiments for applying a superconducting ^{123}Y coating onto the outer surface of CH shells (see Fig. 7b).

The HTSC tapes of SuperOx J-PI-12-20Ag-20Cu type are made on the basis of superconducting epitaxial $GaBa_2Cu_3O_{7-X}$ (or ^{123}Ga) film deposited on a Hastelloy C-276 alloy substrate (nonmagnetic). The width of the tape is 12 mm, the thickness being

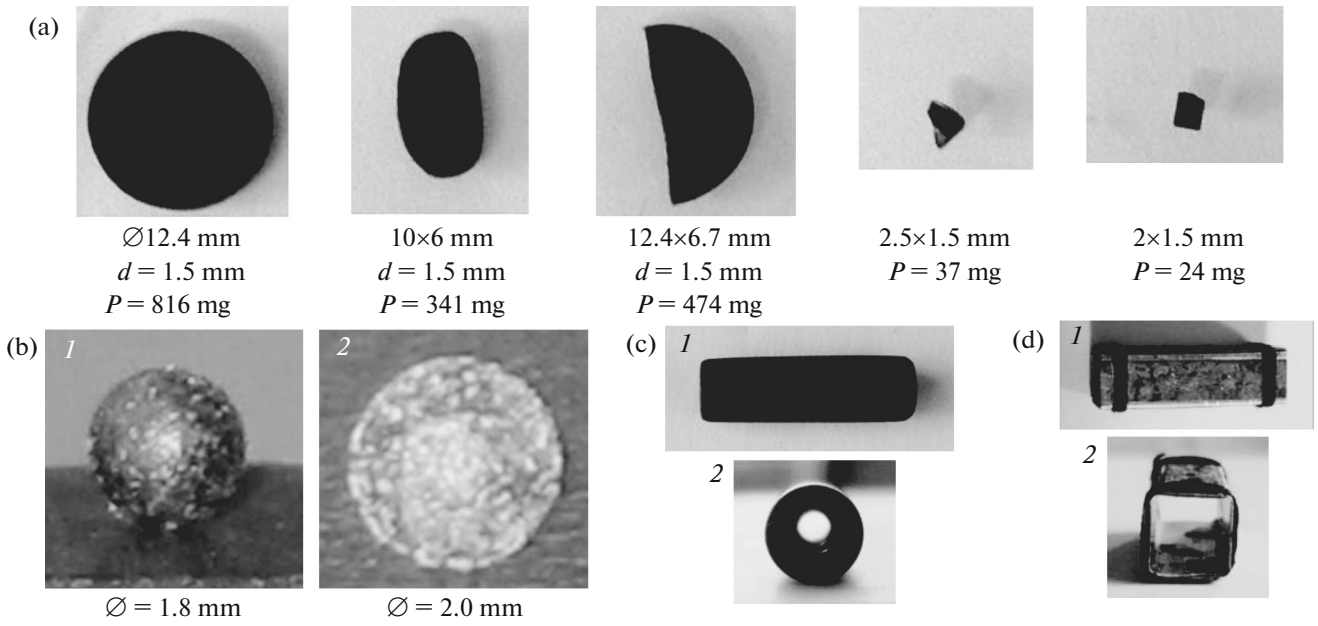

Fig. 7. High-temperature superconducting samples manufactured at LPI for the experimental modeling in the field of target positioning and transport: (a) samples of ^{123}Y ceramic of various shapes and sizes; (b) polymeric shells with an external coating of a composite basing on ^{123}Y powder spread over the polymeric matrix, the target diameter and the coating thickness, respectively, are 1.8 mm and 10 μm (*1*), 2 mm and 50 μm (*2*); (c) sabot made on the basis of ^{123}Y ceramic ((*1*) side view, (*2*) end view), length 16 mm, outer diameter 5 mm, internal diameter 2 mm; (d) sabot manufactured on the basis of HTSC tape produced by JSC SuperOx ((*1*) side view, (*2*) end view, size 20 × 5 × 5 mm, wall thickness 0.28 mm).

0.08 mm, while the thickness of the superconducting film itself is ~1 μm. The critical current for the destruction of superconductivity is $I_c = 425$ A at a temperature $T = 77$ K. The superconducting transition temperature $T_c \sim 92$ K.

To create a HTSC sabot based on the ^{123}Ga tape, four rectangular pieces 20 × 5 mm in size and 0.08 mm thick were cut from the original tape. Then they were fastened on a mandrel of aluminum foil 0.2 mm thick made in the shape of a parallelepiped 20 mm long, 5 mm high, and 5 mm wide (see Fig. 7d). In the experiments, we also used a cylindrical sabot (16 mm long with an outer diameter of 5 mm and internal diameter of 2 mm) made using a turning lathe from a ^{123}Y tablet (see Fig. 7b).

Development and diagnostics of PMG systems. The behavior of ^{123}Y and ^{123}Ga samples with various geometries (for the simulation of both direct and indirect delivery) in magnetic fields of different configuration formed using permanent magnets was studied in detail at LPI in a wide temperature range (from 5 to 80 K). Such systems are called "permanent magnet guideway," or PMG systems. It should be noted that the configuration of the PMG system (Fig. 8) is extremely important for optimizing the transport of HTSC samples from the standpoint of the levitation force, positioning stability, and sample velocity.

In our experiments for the development of PMG systems, we used uncoated neodymium magnets with axial magnetization produced by JSC Midora (Moscow), as well as various inserts made of a ferromagnetic material (E41 grade electrical steel). The measurements of the magnetic field profile in the PMG systems were carried out using a magnetometer made at LPI on the basis of a DKhK-0.5A Hall effect sensor with a sensitivity of 280 mV/T, the range of the measured field being ±1 T, the measurement error amounting to ±0.005 T, and the accuracy of the sensitive element position being 0.1 mm.

Experimental setup. For the investigations in the field of HTSC levitation, a closed-cycle optical helium cryostat made at CryoTrade Co, Moscow, was used, equipped with commercial elements from CryoMech (USA). The cryostat provided a temperature range from 5.3 to 90 K. The temperature measurements were carried out with an accuracy of ±0.1 K using temperature sensors from Lake Shore Cryotronics (USA). A Pfeiffer vacuum pumping system (Germany) and an optical observation system based on a Carl Zeiss microscope with a 10 μm resolution were also used in the experiments (Fig. 9).

A number of model experiments were carried out in an open system (a bath with liquid nitrogen), which allowed one to cool HTSC samples and PMG systems in the temperature range from 77 to 80 K.

Discussion of the results. The experiments carried out near 80 K and at a temperature of 18.5–6 K (see Figs. 8 and 10) demonstrated the efficiency of interaction in an HTSC–PMG pair over a wide temperature

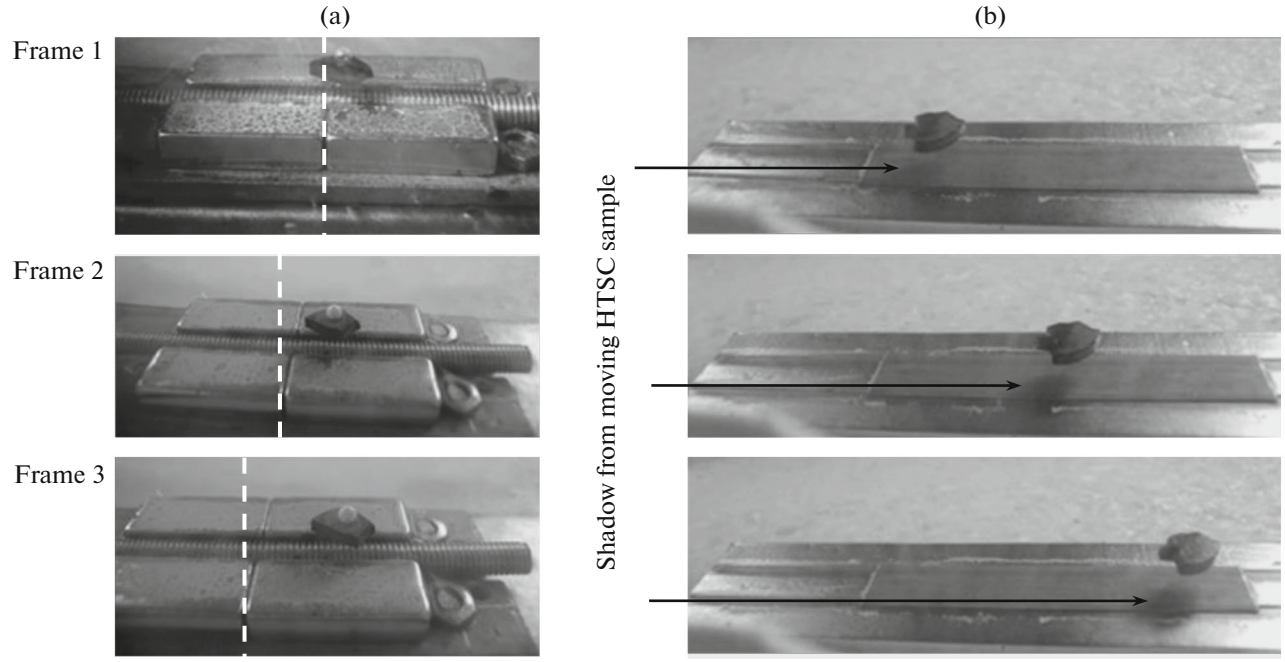

Fig. 8. The simplest PMG systems that allow the implementation of the motion of HTSC samples: (a) PMG system consists of four permanent magnets with a screw ferromagnetic insert placed on a plate of soft magnetic iron (frames 1, 2, and 3 differ in the levitation height of HTSC samples); (b) PMG system consists of three permanent magnets with a magnetically soft iron plate placed on top. The experiments were carried out at a temperature $T = 80$ K.

range, which makes it possible to carry out studies on the motion of a sabot near 80 K, i.e., under the conditions of nitrogen cryogenics (the boiling point of liquid nitrogen $T_{Ne} = 77$ K), rather than helium cryogenics ($T_{He} = 4.2$ K), which is much cheaper.

In the experiments concerning the magnetic levitation (maglev), three types of HTSC sample motion were implemented: the first type consisted in the positioning in a given region of space (Figs. 11, 12), the second type consisted in a linear cyclic motion (Fig. 13), and the third type consisted in a circular cyclic motion (Fig. 14).

The implementation of a stable levitation of HTSC samples in a given region of space is caused by certain properties of HTSC materials belonging to type II superconductors that exhibit an incomplete Meissner effect with a partial field displacement. The field is pushed out completely only when the external magnetic field does not exceed a lower critical value, which, for example, for a superconducting ceramic amounts to 3 mT. At higher fields, the magnetic flux begins to penetrate the sample, which, however, continues to retain superconducting properties until the field reaches an upper critical value. Thus, with increasing magnetic field, a type II superconductor "finds an opportunity" to let the field inside, as if to "freeze" it (pinning effect), while preserving superconductivity. That is, the magnetic flux was captured and stabilized in the HTSC samples, and the achieved effect did not depend on the initial position of the sample (see Fig. 12).

The main conclusions that can be drawn at this stage of our research work are the following:

—A stable levitation of HTSC samples is observed in the case of all types of motion (suspension of a superconductor at a given point in space, cyclic motion of a superconductor either in a linear or in a circular manner). This fully complies with the requirements for the development of a noncontact positioning system and CFT transport into the focus of a powerful laser facility or into an ICF reactor.

—Upon development a "maglev" type delivery system, the HTSC materials can be used both in the design of the CFT coating and in the design of the sabot as a carrier of CFT.

—Let us emphasize that the required levitation force can be achieved under a relatively simple configuration of the PMG system, which greatly simplifies any design developments.

—It is possible to construct a CFT accelerator in such a form where the guide tube of an electromagnetic injector made of HTSC is stationary, whereas a magnetized body (CFT + coating or CFT + sabot) moves along the guide of the injector.

An important observation should be made regarding the influence of the microstructure of the superconductor on the optimization of the performed studies. Common HTSC materials obtained via a solid-

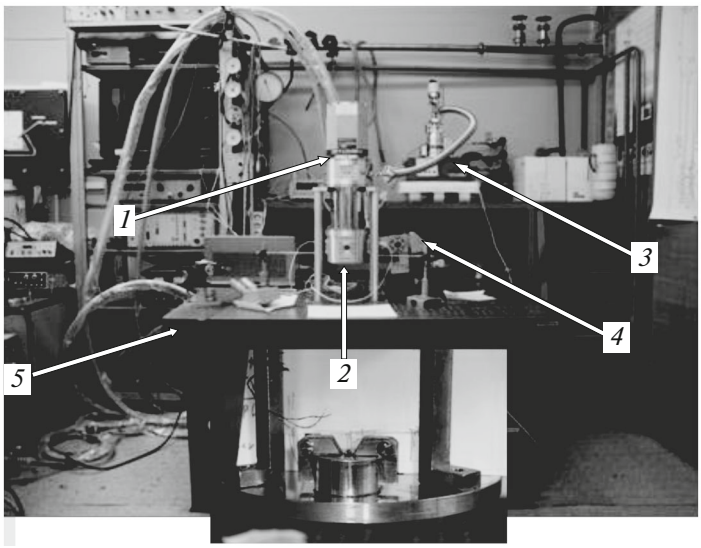

Fig. 9. Setup for the studies on the levitation of HTSC samples: (*1*) cryostat (manufactured by JSC CryoTrade); (*2*) area for placing the PMG system with an HTSC sample (inside the optical chamber of the cryostat); (*3*) vacuuming system by Pfeiffer, Ltd.; (*4*) optical observation system; (5) optical table.

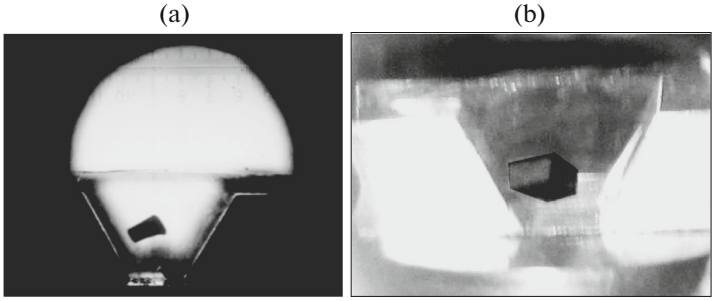

Fig. 10. Behavior of the HTSC–PMG system at $T < 18.5$ K: (a) levitation of an HTSC sample over a magnet, experiments were performed in the temperature range from 6 to 18 K; (b) levitation of a magnet over a HTSC sample, HTSC samples based on ^{123}Y ceramic (produced by LPI) and permanent neodymium magnets (Midora) were used.

phase synthesis represent ceramics where the microscopic crystallites of the HTSC phase are disoriented in space with respect to each other and weakly interconnected between each other (so-called superconducting glass). The potentialities of levitation properties for such materials could be limited. One of the possible ways for obtaining HTSC with a given microstructure consists in crystallizing from the melt, since the diffusion rate of the components in the melt is much higher than it is in the solid. In addition, because of a relatively low viscosity of the melt, it is possible to "adjust" anisotropic crystallites under formation with respect to each other, as the coinciding parts of a mosaic. So, for example, a complex microstructure of HTSC samples was observed by the authors of [23], who revealed many interesting and completely nonrandom features related to macro-, meso-, and microlevels of the material structurization. This creates prerequisites for the formation of an optimal microstructure of a high-temperature superconducting material just for taking into account the specificity of the concrete posed task, in our case, the construction of a "maglev" type delivery device to continuously provide the experiments of the ICF program with cryogenic hydrogen fuel.

Summary. At LPI, research work has been begun concerning the prospects for using the phenomenon of HTSC quantum levitation as a method of contactless CFTs positioning and transport under the delivery thereof to the focus of a high-power laser facility or to an ICF reactor. At this stage of the research work, a superconducting ceramic based on $YBa_2Cu_3O_{7-X}$ with a superconducting transition temperature $T_c = 91$–93 K and also HTSC tape of a SuperOx J-PI-12-20Ag-20Cu type made on the basis of superconducting epitaxial $GaBa_2Cu_3O_{7-X}$ film with a super-

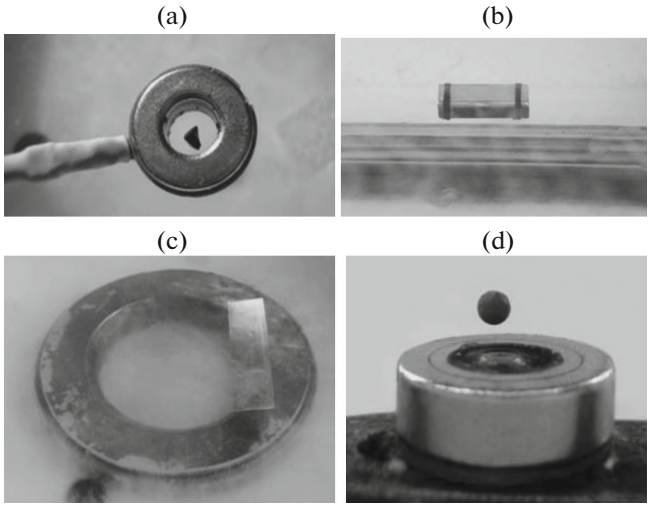

Fig. 11. Positioning of HTSC samples in the magnetic field of different PMG systems: (a) capture and positioning of a ^{123}Y sample in the PMG-2 system; (b) positioning of a sabot made of an HTSC tape produced by JSC SuperOx in the PMG-3 system; (c) positioning of high-temperature superconducting tape produced by JSC SuperOx in the PMG-4 system; (d) capture and positioning of a polymeric shell with an external ^{123}Y coating in the PMG-1 system. The experiments were carried out at $T = 80$ K.

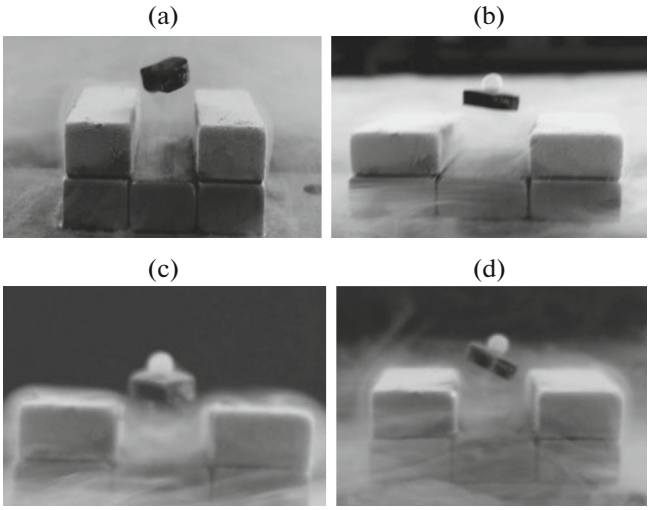

Fig. 12. Use of the pinning effect to stabilize the position of HTSC samples: (a) levitation of an HTSC sample in a magnetic field ($T = 80$ K); (b–d) levitation of an HTSC sample with a polystyrene shell ∅ 2 mm placed on it in a magnetic field. The experiments were carried out at $T = 80$ K.

conducting transition temperature $T_c \sim 92$ K have been used as HTSCs.

In the work it is demonstrated that it is possible not only to implement a stable levitation of different HTSC samples but also to perform a linear and cyclic motion of them. The results will be used in the LPI program for the development of a noncontact CFT delivery system with the use of a linear or cyclic accelerator.

ONLINE CFT CHARACTERIZATION USING HOLOGRAPHIC PATTERN RECOGNITION METHODS

In this section, we discuss one of the promising variants allowing one to perform an ultrafast repeatable characterization of CFT quality and motion trajectory. Since the CFT delivery to the reactor chamber should be carried out at a rate of ~10 targets/s, the characterization method should provide a high repeatability of the quality control process and the implementation of this process during the flight of the CFT injected into the ICF reactor chamber. Preliminary investigations presented in [24] showed that the method of coherent optics based on Fourier holography can be successfully applied to control the parameters of the injected CFT.

Physical principles of the method. The holographic methods for pattern recognition are based on the use of Fourier holograms. A Fourier hologram is a hologram obtained in the back focal plane of a lens as a result of interference of light from two sources located in the input focal plane [25, 26].

Let us consider the arrangement shown in Fig. 15a. A coherent light beam falls from the left on the object and on a small lens that forms a point reference source. They are located in the focal plane of the lens L_1. This plane is called an input or a spatial plane. The back focal plane C of the lens L_1 is called a frequency plane.

The second lens L_2 carries out an inverse transformation; its back focal plane is called an output plane. If there is nothing in the frequency plane, then this optical arrangement gives an inverted image of the object and the reference source in the output plane.

Now let us suppose that we have an object with which we want to compare other objects. Let us arrange it in the input plane, whereas in the frequency plane we place a medium for recording the hologram, for example, a photographic plate. The first lens creates a Fourier transform of the object transmission in the frequency plane. The reference source would give there a plane wave with a phase that changes linearly along the Y axis, as is evident from the geometry of the arrangement shown in Fig. 15a. In the hologram, a result of the interference between the Fourier transform of the object transmission and a plane reference wave would be recorded.

Let us look now what happens if, after registration, we develop the hologram in an appropriate way and place it back into the frequency plane (Fig. 15b). The hologram of the object is created by two waves, an object wave and a reference one. It is well known that in principle these two waves differ in nothing. So, if we remove the object and leave only the reference source, then, in the output plane in the presence of a holo-

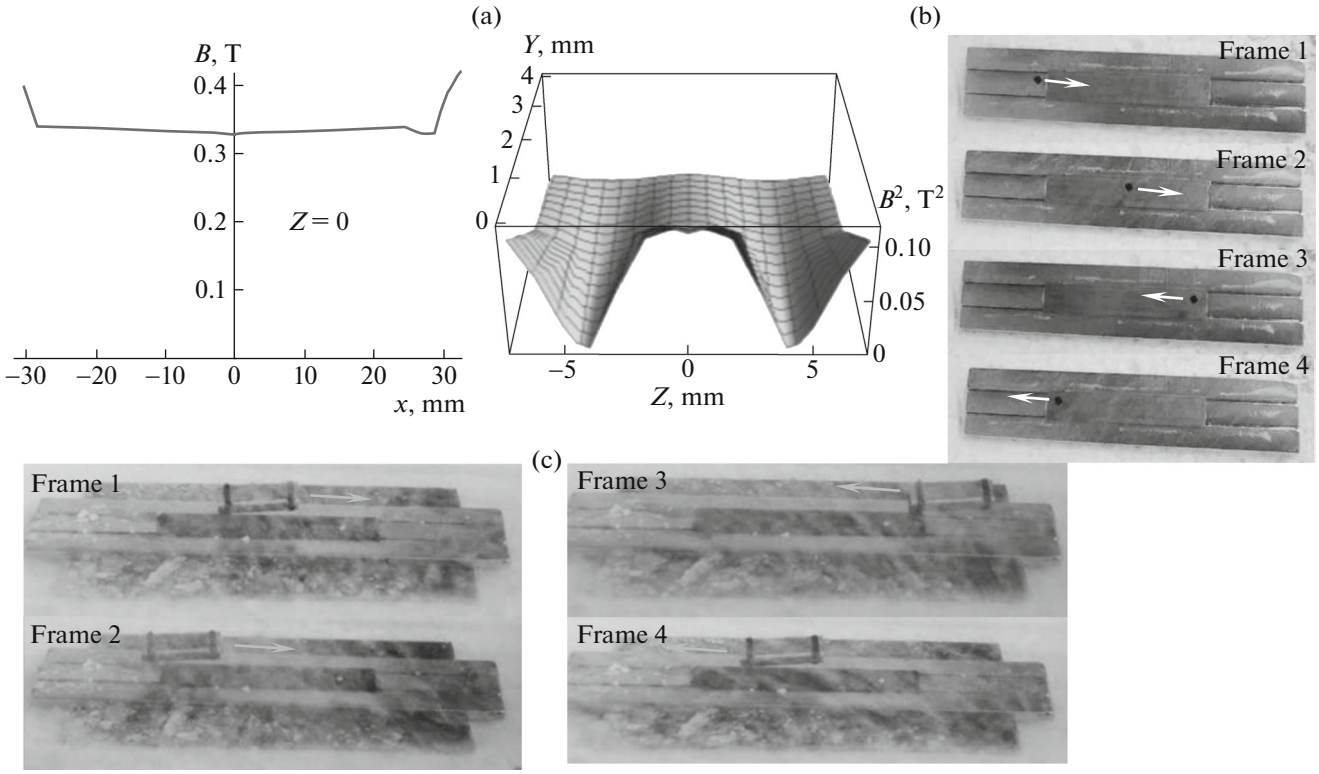

Fig. 13. Implementation of cyclic linear motion of HTSC samples in the magnetic field of the PMG-3 system: (a) magnetic field distribution in PMG-*3;* (b) ^{123}Y sample, size 2 × 1.5 mm; (c) sabot of HTSC tape produced by JSC SuperOx, size 20 × 5 × 5 mm. In photographs (b, c), frames 1–4 are made with a time interval of 0.5 s. The motion was started via gravitational loading. The experiments were carried out at $T = 80$ K.

gram in the frequency plane, an image of the object is formed. In a similar way, if we remove the reference source and leave the object, in the output plane, we obtain an image of the reference source—exactly where it would appear without a hologram in the frequency plane. Since the reference source is pointlike, the intensity distribution in its image represents a sharp peak. It can be further shown that the observed peak represents an autocorrelation function of the object transmission.

Let us now make the last fundamental step. Leaving the hologram of the ideal object obtained in the described manner in the frequency plane and removing the reference source, let us now place another object in the input plane. Then, in the output plane, at the place where we should have the image of the reference source, we obtain a signal proportional to the correlation of the transmission function of the two objects (we shall further call everywhere the transmission function simply "transmission"). This signal is the greater, the more similar are the two objects (but always smaller than the autocorrelation peak).

Thus, such a simple optical arrangement shown in Fig. 15b is capable of comparing two objects. A measure of comparison is the correlation function of two transmissions. Such a scheme is called a correlator with a frequency plane [26].

The mentioned scheme performs a spatial image filtering, and the filter is represented by a hologram. The holographic filter obtained by the described method is called coherent. It should be emphasized that such a filter can be manufactured not only using the described method but also by means of a direct computer synthesis. In this case, we no longer need a real reference object.

In the frequency plane, there occurs multiplying of the Fourier transforms of the transmissions of two objects—the object at the input and the object recorded in the hologram. If we impose another filter (normal, with actual transmission, for example, weakening the higher or lower spatial frequencies) on the holographic filter, then an interesting opportunity arises to compare two objects in a preset band of spatial frequencies. This opportunity seems to be extremely interesting just for the purposes of CFT quality diagnostics. It is possible instrumentally, in a separate manner, to evaluate the contribution of individual spatial frequencies, for example, small-scale inhomogeneities (higher spatial frequencies) or global shape distortions (lower frequencies). In concluding

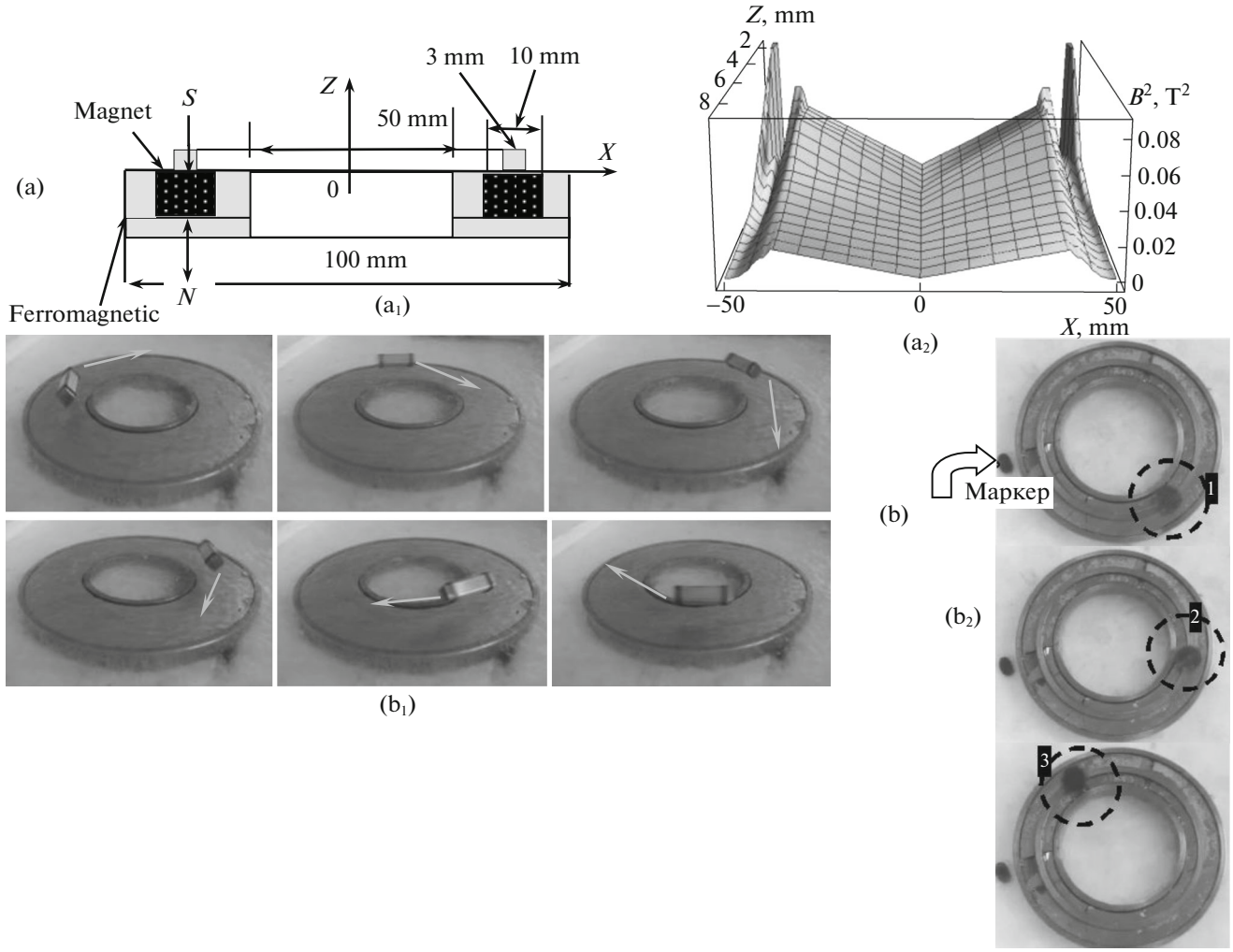

Fig. 14. Implementation of the motion of HTSC samples with respect to the Z axis in the PMG-4 system: (a) configuration of the PMG-4 system that provides a stable circular motion of an HTSC sample with respect to the Z axis (a_1), and the distribution of the square of magnetic field for PMG-4 (a_2); (b) freeze-frame shots of the circular motion of HTSC samples with respect to the Z axis in the PMG-4: rotation of a sabot made of HTSC tape J-PI-12-20Ag-20Cu, rotation velocity 0.5 m/s (b_1); rotation of the ^{123}Y sample, rotation velocity 0.1 m/s (the marker is used as a reference point for fixing the position of the ^{123}Y sample at the moments of time t_1, t_2, t_3) (b_2), the motion was started via a single mechanical impact on the end of the sample. The experiments were carried out at $T = 80$ K.

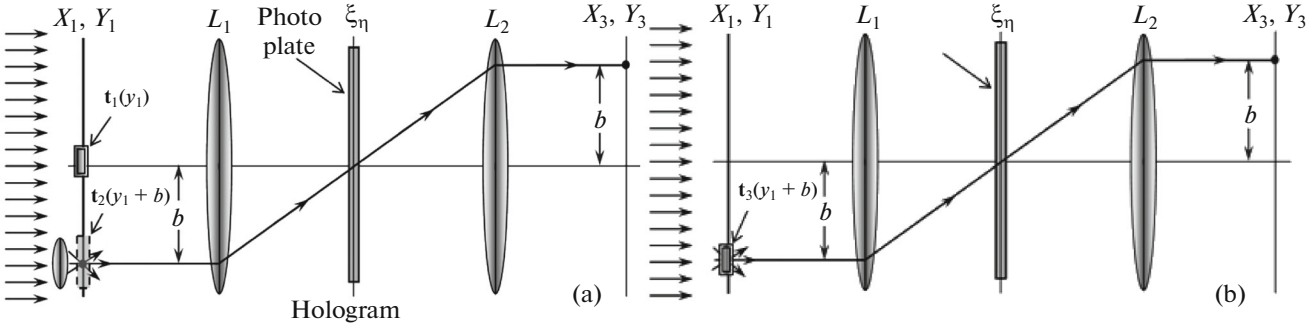

Fig. 15. Optical arrangement of Fourier holography: (a) basic scheme for creating a holographic filter; (b) schematic diagram for the comparison of investigated and reference objects: X_1, Y_1—input plane; ξ_η—frequency plane; X_3, Y_3—output plane; L_1, L_2—lenses; $\mathbf{t}_1(y_1)$—reference object; $\mathbf{t}_3(y_1 + b)$—object under study.

the discussion of the physical aspect of the problem, two more points should be considered:

—Firstly, the scheme presented in Fig. 15 is shown to illustrate the problem and to facilitate the analysis. In principle, it might be forgotten. The only requirement for obtaining Fourier holograms consists in the fact that the object and the reference source should be in the same plane, whereas the identifiable object should be in the same place as the reference one upon obtaining a coherent filter. The relative location of the object, lenses, and holograms can be almost arbitrary; moreover, the lens can simply be thrown out. In all these cases, we obtain equivalent schemes. A detailed analysis of the equivalence of such schemes was carried out, for example, in [25]. This fact means that a real experimental optical arrangement can be designed for reasons of convenience of a specific physical experiment and taking into account the geometry of a real installation.

—Secondly, in Fourier holography, it is assumed that the object is a flat transparency. Only in this case is it possible to obtain a precise Fourier transform and, accordingly, to accurately reconstruct the object from its hologram. However, laser targets have a spatial extent. Nevertheless, it seems to us that this circumstance is not a fundamental obstacle to the proposed method. In support of this statement, there are several arguments.

The length of a target along the optical axis can be much smaller than the focal length of the first lens. This is easy to implement in practice, since the characteristic size of the target amounts to a few millimeters. Consequently, in the first approximation, the object can be considered flat.

In the method under consideration, we are not interested in the exact reconstruction of an object from its hologram. The problem consists in comparing the wave fronts formed by a tested object and a reference object, more precisely speaking, in comparing the axial symmetry and the spatial spectra of these two fronts. The three-dimensionality of the object can be considered here as an additional obstacle that can be compensated by introducing additional filters and optical elements into the optical arrangement.

Mathematical foundations of the method. Let us again consider Fig. 15. Let us denote the complex transmission of our object in the input plane as $\mathbf{t}_1(y_1)$, considering the reference source as the second transparency with a complex transmission $\mathbf{t}_2(y_1 + b)$. It is obvious that, in the case of a point source, this is the delta function $\delta(y_1 + b)$—here it is a spatial analog of a pulse. To simplify the subsequent expressions, we may assume without loss of generality that all the variables depend on one coordinate.

Let us introduce the following notation: an asterisk over a variable name means complex conjugation, F and F^{-1} are the direct and the inverse Fourier transform, and i denotes the imaginary unit.

If the input plane is illuminated by a plane wave of unit amplitude, then the transmitted light has in this plane a complex amplitude

$$\mathbf{t}_1(y_1) + \mathbf{t}_2(y_1 + b). \tag{11}$$

In the frequency plane, the complex amplitude is

$$\mathbf{T}_1(\eta) + \mathbf{T}_2(\eta)\exp(-2\pi i\eta b), \tag{12}$$

where $\mathbf{T}_1(\eta)$ and $\mathbf{T}_2(\eta)$ are the Fourier transforms of transmissions $\mathbf{t}_1(y_1)$ and $\mathbf{t}_2(y_1)$, respectively. In (12), the operation of Fourier transform shift is used. If we register in a linear manner the intensity of a light wave in the frequency plane $\xi\eta$, then the recording medium after the developing will have a transmission t_H, proportional to the given intensity:

$$\begin{aligned} t_H &\sim \mathbf{T}_1\mathbf{T}^* + \mathbf{T}_1\mathbf{T}_2^* \exp(+\pi i\eta b) + \mathbf{T}^*\mathbf{T}; \\ t_H &\sim \mathbf{T}_1\mathbf{T}_1^* + \mathbf{T}_2\mathbf{T}_2^* + \mathbf{T}_1\mathbf{T}_2^* \exp(+2\pi i\eta b) \\ &\quad + \mathbf{T}_1^*\mathbf{T}_2 \exp(-2\pi i\eta b). \end{aligned} \tag{13}$$

Let us now illuminate the resulting hologram with a transmission t_H by a light wave with a complex amplitude $\mathbf{T}_3(\eta)$. Then the complex amplitude of the wave transmitted through the hologram will amount to $\mathbf{T}_3 t_H$. Of our particular interest is the last term in the expression for t_H, since just it gives the image of transparency $\mathbf{t}_2(y_1 + b)$. The complex wave amplitude corresponding to this term in the $\xi\eta$ plane is proportional to

$$\mathbf{T}_3\mathbf{T}_1\mathbf{T}_2\exp(-2\pi i\eta b). \tag{14}$$

The complex amplitude $\mathbf{a}(y_3)$ in the output plane caused by this term is proportional to its inverse Fourier transform

$$\mathbf{a}(y_3) \sim F^{-1}[\mathbf{T}_3\mathbf{T}_1\mathbf{T}_2\exp(-2\pi i\eta b)]. \tag{15}$$

If we now recall that the Fourier transform of the cross-correlation of two functions is the product of the complex conjugate Fourier transform of one function and the Fourier transform of the other, then the product $\mathbf{T}_3\mathbf{T}_1^*$ can be written in the form

$$\mathbf{T}_3\mathbf{T}_1^* = F[\mathbf{t}_3^*(y_3)\mathbf{t}_1(y_3)]. \tag{16}$$

Then $\mathbf{a}(y_3)$ takes the form

$$\mathbf{a}(y_3) \sim F^{-1}\{F[\mathbf{t}_3^*(y_3)\mathbf{t}_1(y_3)]\mathbf{T}_2\exp(-2\pi i\eta b)\}. \tag{17}$$

Since $\mathbf{T}_2\exp(-2\pi i\eta b)$ represents $F[\mathbf{t}_2(y_3 + b)]$, then, using the theorem of convolution, we obtain

$$\begin{aligned} \mathbf{a}(y_3) &\sim F^{-1}\{F[\mathbf{t}_3^*(y_3)\mathbf{t}_1(y_3)]\mathbf{T}_2 \exp(-2\pi i\eta b)\} \\ &\sim [\mathbf{t}_3^*(y_3)\mathbf{t}_1(y_3)]\mathbf{t}_2(y_3 + b). \end{aligned} \tag{18}$$

From expression (18), it is immediately seen that the complex amplitude in the output plane is the convolution product of the transmission function $\mathbf{t}_2(y_3 + b)$ of one object (reference) with the correlation of transmission $\mathbf{t}_3(y_3)$ of the object under study and the transmission $\mathbf{t}_1(y_3)$ of the reference object fixed in the hologram. If $\mathbf{t}_2(y_3 + b) = \delta(y_1 + b)$, which means that a

point source is used as the reference, then at the output we have a signal proportional to the correlation of the two transmissions (this directly follows from the properties of a convolution product). We can also see that the correlation peak will be observed at that point in the output plane where there should be a reference source image in the absence of the filter in the frequency plane.

Thus, a simple mathematical analysis of the optical arrangement [24–26] unambiguously indicates the possibility to compare two objects. In addition, the written simple formulas can be directly applied to numerical model calculations, which we have just used.

Implementation of the model. To test the sensitivity of the proposed scheme with respect to the distortion of the target, its numerical model has been developed. Shadow images of targets considered as amplitude transparencies come to the input of the model. The algorithm of the model is based on the relationships presented in the previous section. Then, the model provides for additional functions. Let us list the main features of the model:

1. Obtaining and visualization of a cross-correlation matrix for two input images (autocorrelation matrix, when these images are identical).

2. Measurement and output of the correlation peak amplitude. The amplitude can be both measured at one point (maximum) and averaged over a circle of a given radius.

3. Modeling of obtaining an object image from its Fourier hologram using a point reference source. The size and position of the source can be set arbitrarily.

4. Spatial filtering of images using filters of low and high frequencies, as well as a rejection filter, i.e., a filter that does not transmit oscillations having a certain frequency band, but transmits oscillations with frequencies beyond this band. The boundaries of the filters in the frequency domain can be set arbitrarily.

5. Measuring a correlation between two images in combination with the application of spatial filters and independently for each of the two images.

6. Possibility to simulate pattern recognition holographic systems.

7. Visualization of the power spectrum of the Fourier image along any scanning line passing through the zero mode.

In practice, the model is embodied in the form of the Hologram complete computer code that operates in a Windows environment. To perform a fast two-dimensional Fourier transform, a FFTW library is used therein [27]. The computer experiments carried out using the Hologram code demonstrated an ability to monitor the quality of both a single CFT and a CFT array using Fourier holography (Figs. 16a, 16b, and 17) and to diagnose deviations in the shape of CFT in the range of high, medium, and low harmonic components (Fig. 18).

Discussion of the results. Using the Hologram code, a study was performed concerning the sensitivity of the circuit shown in Fig. 15 with respect to distortions in the CFT shape. These are global distortions, such as a shift of the inner surface with respect to the center (see Fig. 18a)—they correspond to low and middle spatial frequencies; and small-scale distortions, such as the roughness of the inner surface (Fig. 18b)—they correspond to the highest spatial frequencies. As it was shown in [24], the distortions in the shape of the inner surface of the cryogenic layer lead to a shift or distortion in the shape of the bright ring. Several sets of images of a cryogenic fuel target were produced as the inputs for the Hologram code (the outer shell thickness being 0.07, the thickness of cryogenic fuel layer being 0.12 parts of the outer radius of the target). The size of these images was 1010 × 1010 pixels. The test images were made via selecting the radial distribution of the intensity closest to the real one, as well as taking into account the data of optical modeling [28].

Let us first consider how the shift of the inner surface center of the cryogenic layer affects the value of the correlation peak (see Fig. 18a). In this figure, the amplitudes are normalized to the amplitude of the autocorrelation peak of an undistorted image. In addition, the first two spatial-frequency modes have been removed. Let us recall that the zero Fourier mode is simply proportional to an average illumination level. One can see that the sensitivity of the circuit with respect to such distortions is high and amounts to approximately 7% per 1% of the relative shift. In fact, the shift determined in this manner corresponds to a polythickness expressed in percentage. From Fig. 18a, one can see that the curves obtained at a large noise level are shifted downward. This does not reflect any physical phenomenon, being connected only with the incorrectly normalized data in the presence of strong noises. The two these curves are presented here to show that, even at a very strong noise, the tendency of the correlation peak amplitude to decrease with increasing asymmetry of the target is well manifested. It should be noted that the noise with a variation of 20% is a very large noise and it is even difficult to obtain it in practice, except for speckles.

Another set of input data contained images corresponding, generally, to a symmetric cryogenic target. The inner surface of this target, however, was distorted by a sinusoidal wave (the hundredth mode on the circumference of the inner surface). Figure 18b shows the obtained results. It can be seen that, if the intensity of the correlation peak is measured under the same conditions as before, the sensitivity is low. It is obvious that, if we are looking for high-frequency distortions, then the lower spatial modes are only hindering. Indeed, the use of a high-frequency spatial filter makes it possible to obtain a much better result.

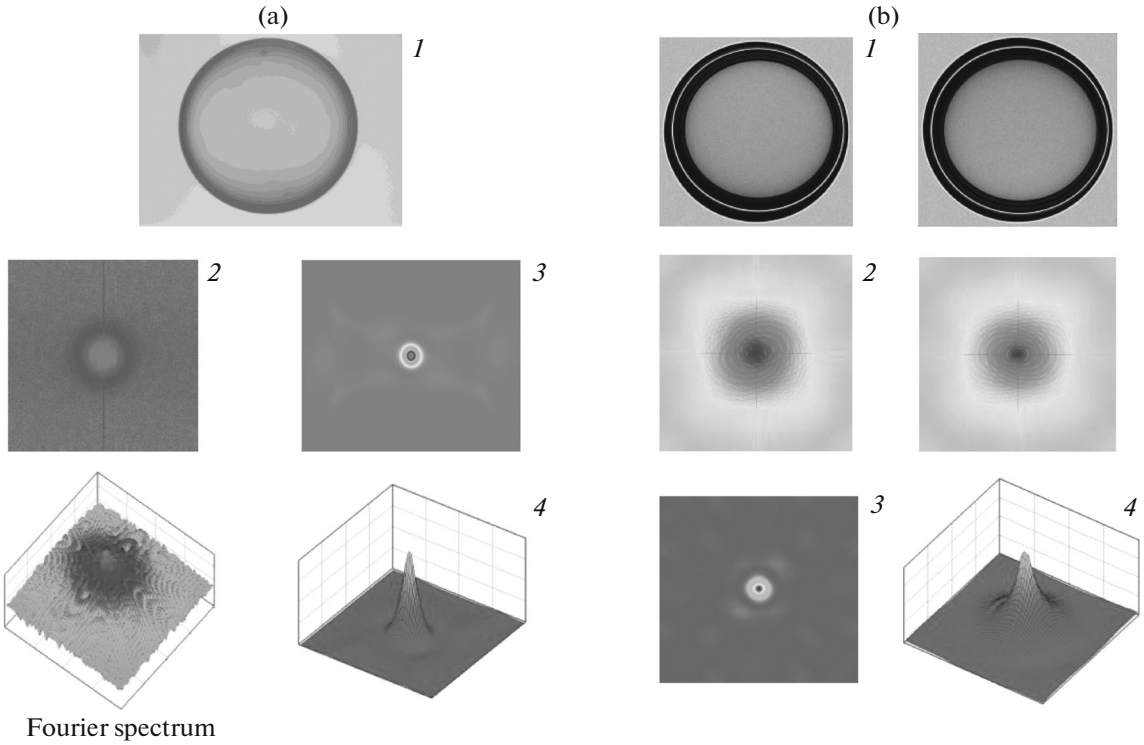

Fig. 16. Two examples of the Hologram code: (a) shadow image of a real single-layer shell (*1*), Fourier spectrum of this image (*2*), autocorrelation matrix presented in conventional colors (*3*) and that presented as a three-dimensional graph (*4*); (b) simulated images of two slightly differing bilayer shells (*1*), corresponding Fourier spectra of these shells (*2*), cross-correlation matrix of images presented in conventional colors (*3*) and that presented as a three-dimensional graph (*4*). Modeling of images was carried out using a specialized Shell Optics Model software package developed at LPI [28]. The calculation is made for 120×10^6 beams.

The results obtained at different noise levels are given in Table 2, which shows the relative sensitivity expressed as a percentage of 0.001 amplitude distortion, i.e., 1% means that the amplitude of the correlation peak changes by 1% when the distortion amplitude changes by 0.001 R_{out}.

The presented results show that the scheme using Fourier holography exhibits a good sensitivity with respect to target distortions both in high and in low harmonics (see Figs. 18a, 18b). Moreover, this scheme allows one to perform the quality control not only for a single target (see Figs. 16a, 16b) but also for a target array (see Figs. 17a–17c).

Measurement of the CFT velocity and trajectory. When the CFT is injected into the reactor chamber, it is necessary to control the two most important parameters: the velocity of the CFT and its trajectory in the chamber. In this case, it is advantageous to use a strategy where all measurements are made simultaneously. In this section, we consider the solution of this problem. For definiteness, let us consider the velocity of the CFT to be in the range from 200 to 400 m/s, which is typical of a commercial power station. Figure 19 shows a scheme based on the further development of the proposed idea.

Let the CFT move from top to bottom in the input plane (see Fig. 19, left) and pass a distance S_{in} from position I to position II in time t. The diaphragm with two holes is located between the light source and the CFT plane. The diameter of each hole is slightly larger than the diameter of the CFT; the distance between their centers is S_{in}. The figure shows one light source, but it is also possible to use two light sources, one for each position of the CFT. In the output plane, the correlation maximum moves in the direction opposite to the direction of the CFT motion, i.e., bottom to top. If

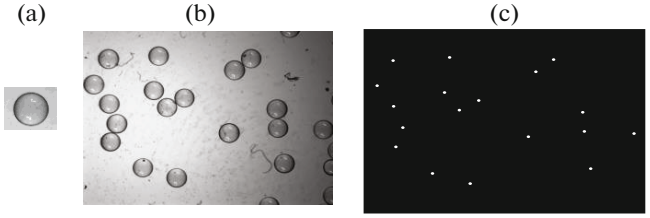

Fig. 17. Recognizing an array of shells using the Hologram code: (a) single-layered shell as a reference image; (b) image of the studied array of single-layered shells; (c) cross-correlation matrix, correlation peaks correspond to the location of the shells in image (b).

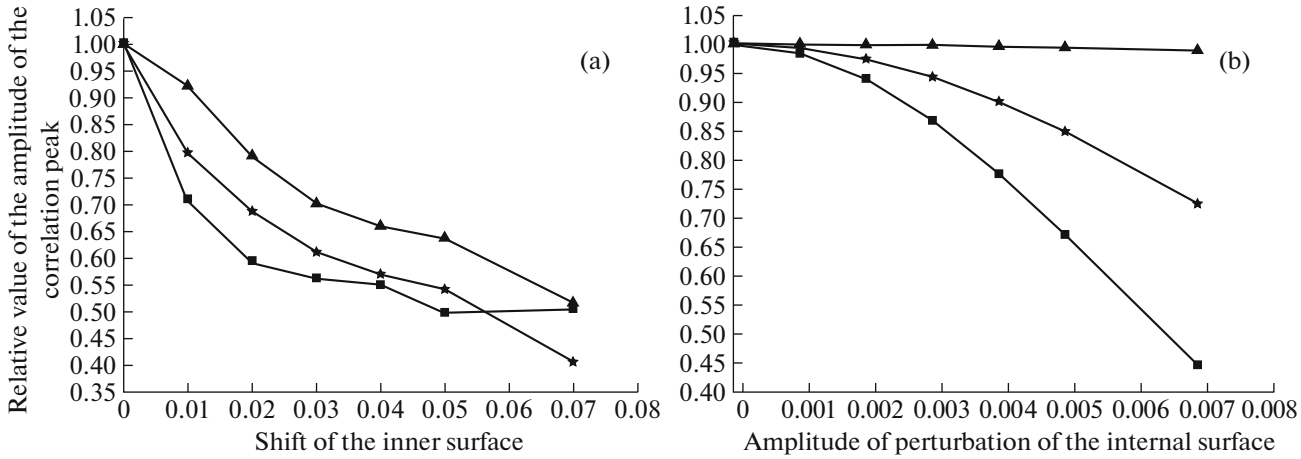

Fig. 18. Investigation of the sensitivity of the holographic arrangement to various noise levels using the Hologram code: (a) recognition of disturbances in low modes (layer polythickness), relative amplitude of the correlation peak, (—) shift of the inner surface of the cryogenic target (normalized to the outer CFT radius): (▲) Gaussian noise RMS = 2%; (★) speckle noise RMS = 20%; (■) Gaussian noise RMS = 20%; (b) recognition of disturbances in high modes (roughness of the layer), relative value of the amplitude of the correlation peak, (—) the perturbation amplitude of the CFT internal surface under three different modes of spatial filtration (normalized to the value of the CFT outer radius): modes 0 and 1 are excluded (▲); modes from 0 to 30 are excluded (★); modes from 0 to 60 are excluded (■).

the configuration of the CFT is close to the reference configuration (namely, this case is of interest to us), then the correlation peak is quite intense and narrow. In the output plane of the optical arrangement (this is the plane of detectors), two photodiodes D_1 and D_2 are located at a distance S_{out} from each other, as well as two fast CCD arrays LA_1 and LA_2.

The CCD arrays are located near the photodiodes in a plane perpendicular to the optical axis and along the line that is perpendicular to the CFT trajectory (Fig. 20). The distance S_{out} is chosen so that, during the CFT movement from position I to position II, the correlation peak moves from D_1 to D_2. It is clear that the distance S_{out} can always be determined for a particular optical arrangement. The time delay t measured between the signal peaks of the first and second detectors unequivocally determines the value of CFT velocity $V = S_{in}/t$. Here it is assumed that the CFT moves evenly. If this is not the case and the CFT moves with acceleration, the measurement scheme becomes

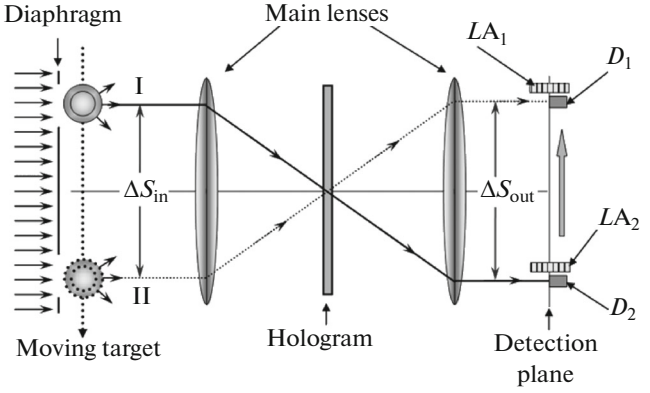

Fig. 19. Scheme that allows simultaneously determining the quality, velocity, and trajectory of a moving target.

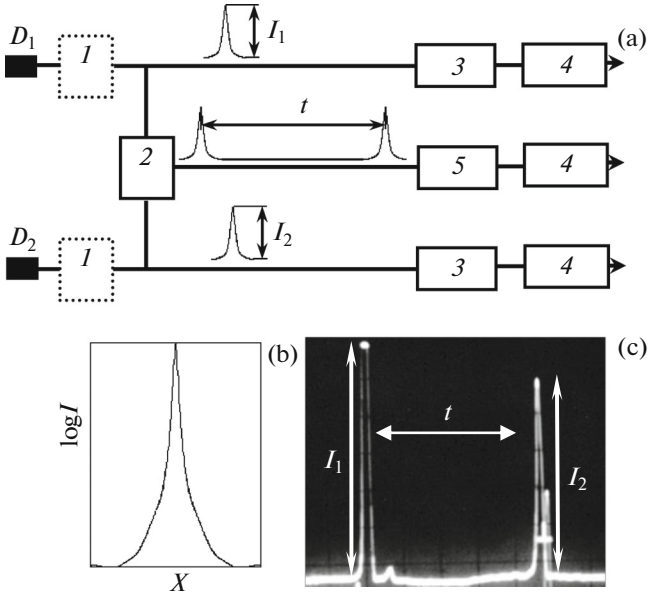

Fig. 20. Diagram of the electronic unit designed to diagnose the target quality and velocity: D_1 and D_2—photodetectors; (*1*) amplifier; (*2*) analog totalizer; (*3*) analog-to-digital converter (ADC); (*4*) digital comparator for input and reference data; (*5*) time-to-digital converter (TDC) (a); profile of the calculated correlation peak (b); oscillograms of signals obtained during the experimental simulation of the electronic circuit operation (c).

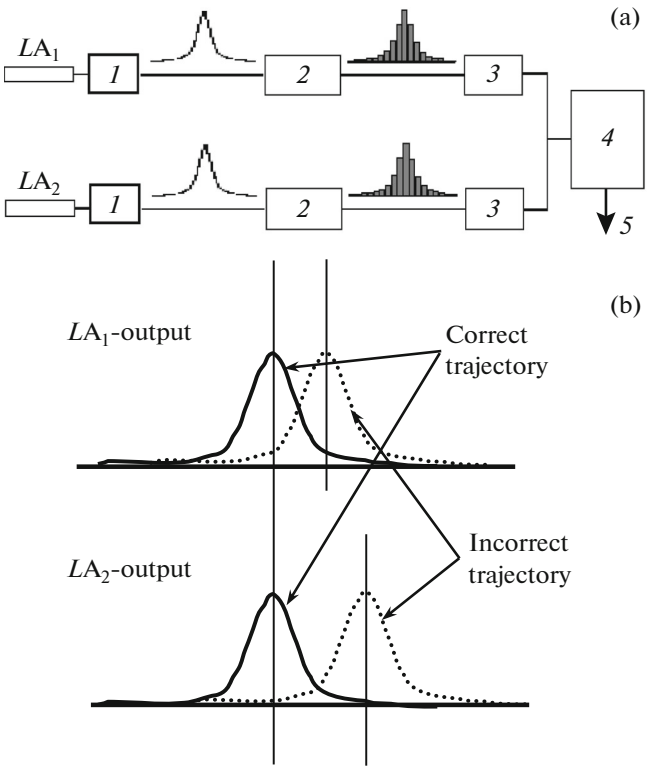

Fig. 21. Determination of the target trajectory: (a) block diagram of electronic equipment for determining the target trajectory: LA_1 and LA_2—CCD arrays; (*1*) amplifier; (*2*) analog-to-digital converter (ADC); (*3*) buffer memory; (*4*) processor; (*5*) output signal; (b) schematic diagram by means of which a target velocity vector can be determined.

somewhat more complicated (in this case, it should involve three or more detectors), and the algorithm for the calculation of the CFT velocity changes in a corresponding manner. However, this is not fundamental, and we do not consider such variants herein.

The schematic diagram shown in Fig. 20 illustrates a possible technical solution for simultaneously determining the velocities of CFTs and selecting them for quality. It can be seen that the CFT velocity can be determined immediately, as soon as it passes point II. Let the distance between points II and I be 3 cm. Therefore, the CFT needs about 10^{-4} s to overcome this distance. Such a time interval can be easily measured with a high accuracy. For example, if the frequency of the master oscillator is 10^9 Hz, then the measurement accuracy amounts to 10^{-3}%. A possible circuit of the electronics module for the analysis of CFT trajectory and the development of a control action on it is shown in Fig. 21.

Table 2. Amplitude of CFT shape deviation from the ideal one at a different noise level

Noise level	Modes >1	Modes >30	Modes >60
Gaussian noise 2%	0.17	4.5	9.1
Speckle noise 20%	0.18	4.5	9.4
Gaussian noise 20%	*	3.6	7.1

* No reliable measuring is possible, too much data scattering.

It should be noted that earlier we considered the determination of CFT trajectory only in one plane, since it is obvious that two identical orthogonal schemes are needed to determine its trajectory in space.

Summary. The development of online characterization using holographic pattern recognition techniques is a promising direction in the field of CFT quality control, since the speed of the circuit on its basis is on the order of a few microseconds (let us recall that the minimum time of CFT flight in the SOMBRERO reactor chamber amounts to 16 ms). The computer experiments performed at LPI have demonstrated that this approach allows researchers simultaneously to measure the quality of the cryogenic layer and to monitor the dynamics of quality changes, as well as to characterize the velocity and trajectory of moving CFT during its flight in the ICF reactor chamber.

CONCLUSIONS

At LPI, an original concept of a cryogenic target factory (CTF-LPI) is proposed for a continuous formation of cryogenic fuel targets (CFT) and their injection into an ICF reactor chamber at a required rate. The concept has the following distinctive features: the use of FST technologies for an in-line production of CFTs; the use of a quantum levitation of high-temperature superconductors in the magnetic field aiming at the construction of "maglev" type delivery systems for a contactless manipulation, positioning, and transport of CFTs; the use of Fourier holography in the system of online characterization of moving CFTs. This paper presents the results of a large-scale series of experimental and theoretical studies demonstrating that a unique scientific, engineering, and technological base has been developed in Russia for constructing a pilot plant in the scope of the CTF-LPI concept.

Let us recall that, an efficient operation of a power plant using nuclear fusion reactions in the scope of ICF systems requires a high-rep-rate and mass production of CFTs with a rate of $\nu \sim 10$ Hz (according to some data, this rate can be increased already up to ~15 Hz [7]). Therefore, the task of CTF consists in a mass and cheap production of the required number of CFTs which provides a continuous sequence of thermonuclear microexplosions resulting in a positive energy yield.

The most economically attractive variants of such a power plant can be represented by multimodule structures, where one driver serves several reactor modules. To do this, it is necessary that the CTF carry out the

production of fuel units—CFTs—"in a conveyor manner," i.e., the CTF should be able to efficiently work with N reactors according to a scheme such as "one driver–one target factory–N reactors." The conveyor method for the production of the required number of CFTs can be based only on the operation with moving free-standing shells. The efficient solution of this problem would enable one to master an environmentally friendly, safe, and almost inexhaustible source of energy. At the same time, it should be emphasized that the practical use of the inertial driver is possible both in an independent variant and in the framework of the development of a hybrid plant for the production of electric power using chain fission reactions and nuclear fusion reactions.

At the present time, namely the FST technique is the only method in the world based on the operating principle of moving free-standing shells, which provides the production of CFTs in a continuous mode, as well as the supply of finished CFTs simultaneously to several reactor modules. Thus, the FST layering method is applicable to scaleup to reactor CFT production at low cost and the development of the world's first conveyor CTF, which could advance the ICF as a generating platform for energy engineering for a long-term outlook.

ACKNOWLEDGMENTS

The results discussed in the section "HTSC Application to the System of CFT Delivery into ICF Reactor" were obtained in the framework of the project of the Russian Foundation for Basic Research no. 15-02-02947.

We are grateful to the specialists at the LPI Superconductivity Laboratory for their participation in the preparation of HTSC samples from superconducting $YBa_2Cu_3O_{7-X}$ ceramic.

REFERENCES

1. I. V. Aleksandrova, E. R. Koresheva, O. N. Krokhin, and I. E. Osipov, Vopr. At. Nauki Tekh., Ser.: Termoyad. Sintez **38** (1), 57 (2015).
2. I. V. Aleksandrova, E. R. Koresheva, O. N. Krokhin, and I. E. Osipov, Vopr. At. Nauki Tekh., Ser.: Termoyad. Sintez **38** (2), 75 (2015).
3. I. V. Aleksandrova, E. R. Koresheva, O. N. Krokhin, and I. E. Osipov, Vopr. At. Nauki Tekh., Ser.: Termoyad. Sintez **38** (3), 59 (2015).
4. I. V. Aleksandrova, E. R. Koresheva, O. N. Krokhin, and I. E. Osipov, Vopr. At. Nauki Tekh., Ser.: Termoyad. Sintez **38** (4), 51 (2015).
5. S. O. Kucheev and A. V. Hamza, J. Appl. Phys. **108**, 091101 (2010).
6. I. V. Aleksandrova, E. R. Koresheva, E. L. Koshelev, et al., Vopr. At. Nauki Tekh., Ser.: Termoyad. Sintez, No. 3, 27 (2007).
7. National Research Council, *An Assessment of the Prospects for Inertial Fusion Energy, Report* (Natl. Academy, Washington D.C., 2013).
8. I. V. Aleksandrova, A. A. Belolipetskii, E. R. Koresheva, et al., Vopr. At. Nauki Tekh., Ser.: Termoyad. Sintez, No. 4, 22 (1000).
9. E. M. Bringa, A. Caro, M. Victoria, et al., Miner., Met. Mater. Soc. **57** (9), 67 (2005).
10. D. T. Goodin, N. B. Alexander, L. C. Brown, et al., in *Proceedings of the 3rd IAEA RCM on Physics and Technology of IFE Targets and Chambers, Daejon, Rep. Korea, October 11–13, 2004*. http://aries.ucsd.edu.
11. HiPER Software. http://www.hiper-laser.org/.
12. R. Wanner and H. Meyer, Phys. Lett. A **41**, 189 (1972).
13. I. V. Aleksandrova, E. R. Koresheva, I. E. Osipov, et al., J. Russ. Laser Res. **28**, 207 (2007).
14. I. V. Aleksandrova, A. A. Belolipetskiy, E. R. Koresheva, et al., J. Russ. Laser Res. **29**, 419 (2008).
15. I. V. Aleksandrova, A. A. Belolipetskiy, E. R. Koresheva, and S. M. Tolokonnikov, Laser Part. Beams **26**, 643 (2008).
16. S. Nakai and J. Miley, *Physics of High Power Laser and Matter Interactions* (Word Scientific, Singapore, 1992).
17. W. Meyer, in *Proceedings of the 3rd IAEA RCM on Physics and Technology of IFE Targets and Chambers, Daejon, Rep. Korea, October 11–13, 2004*. http://aries.ucsd.edu.
18. E. R. Koresheva, I. E. Osipov, and I. V. Aleksandrova, Laser Part. Beams **23**, 563 (2005).
19. R. Tsuji, Fusion Eng. Des. **81**, 2877 (2006).
20. T. Kassai and R. Tsuji, J. Phys.: Conf. Ser. **112**, 032047 (2008).
21. I. V. Aleksandrova, O. M. Ivanenko, V. A. Kalabukhov, et al., J. Russ. Laser Res. **35**, 151 (2014).
22. I. V. Aleksandrova, A. A. Akunets, P. I. Bezotosnyi, I. S. Blokhin, S. Yu. Gavrilkin, O. M. Ivanenko, E. R. Koresheva, E. L. Koshelev, K. V. Mitsen, and L. V. Panina, Bull. Lebedev Phys. Inst. **42**, 309 (2015).
23. E. A. Gudilin and N. N. Oleinikov, Sverkhprovodimost': Issled. Razrab., Nos. 5–6, 81 (1995).
24. E. R. Koresheva, A. I. Nikitenko, I. V. Aleksandrova, et al., Nucl. Fusion **46**, 890 (2006).
25. R. J. Collier, C. B. Burkhardt, and L. H. Lin, *Optical Holography* (Academic, New York, London, 1971).
26. D. Casasent, in *Handbook of Optical Holography,* Ed. by H. Caulfield (Academic, New York, 1979), Chap. 10, p. 503.
27. FFTW User Manual. http://www.fftw.org/.
28. E. R. Koresheva, I. E. Osipov, I. V. Aleksandrova, et al., J. Russ. Laser Res. **28**, 163 (2007).

Translated by O. Polyakov